1977, *Astron. Astrophys. Suppl.* **30**, 145-168.

H_2O IN THE GALAXY: SITES OF NEWLY FORMED OB STARS

R. GENZEL and D. DOWNES
Max-Planck-Institut für Radioastronomie, Bonn
Federal Republic of Germany

Received April 29, 1977

Positions and spectra are presented for 82 water vapor sources at 22 GHz. Of this list, 32 sources are new discoveries, and nearly all of the sources probably come from expanding shells around newly formed, massive stars.
The H_2O sources can be classified by the appearance of their spectra. Many of the sources have a remarkable symmetry in their low velocity emission, and 14 ($\sim$50%) of the strongest sources show weak, high velocity features extending over ± 25 to ± 260 km s^{-1} around their low velocity lines. The frequency of occurrence of such sources indicates that high velocity emission occurs over a large part of the H_2O phase of stellar evolution.
The luminosity function of the sources has its median at $10^{29.5}$ erg s^{-1} emitted in the H_2O line, with a standard deviation of one order of magnitude. The intensity variations of line features which are near to each other in velocity suggest a "mode switching" phenomenon.
The H_2O sources are near, but do not coincide with, the compact HII regions mapped to date. There are two types of infrared and OH maser sources. The first type is associated with the HII regions, and the other type is directly related to the H_2O sources, on the basis of coincidence in position and velocity.
The OH maser lines which are related to H_2O sources come from the red or blue shifted parts of a circumstellar shell, at the same velocities as the H_2O emission.
We discuss briefly a possible arrangement of certain H_2O sources in an evolutionary sequence.

Key words: H_2O masers – star formation – infrared sources – compact HII regions – stellar winds

1. INTRODUCTION

The H_2O maser lines at 22 GHz seen in the vicinity of HII regions are probably emitted in dense, hot (10^2 to 10^3 K) shells or disks around massive stars in the later stages of their formation. The evidence for this interpretation is as follows:

i) Very long baseline interferometry shows that H_2O masers cluster in "centers of activity" of 10^{16} cm size–about the scale expected for the dust shells of newly formed OB stars.

ii) About half of the H_2O sources presented in this paper have a characteristic "double" or "triple" symmetry in their spectra which is suggestive of maser emission from the front and rear sides of an expanding shell or disk. The patterns are similar to those in OH spectra of late-type stars, where the symmetry is even more striking (Reid *et al.* 1977, Moran *et al.* 1977a, Olnon 1977, Dickinson 1976).

iii) These symmetrical velocities of 10 to 20 km s^{-1} over 10^{16} cm are difficult to interpret with any model other than an expanding disk or shell. Models involving contraction or rotation require improbably high central masses. A detailed discussion of this point with respect to the dominant low velocity H_2O emission in Orion is given in Genzel and Downes (1977).

iv) The high luminosities of the H_2O sources considered here–typically of the order of 10^{-4} $L_\odot$ in a 100 KHz wide line at 22 GHz–suggest that the ultimate energy sources must be massive stars, *i.e.,* OB stars. It also means that with our current sensitivity, we should be able to find every newly born O star in the Galaxy.

These facts, together with the ability to map the sources over scales of 10^{13} to 10^{17} cm, by means of VLBI, make maser radiation one of the best probes of regions of star formation.

We have started a survey for water vapor sources in the vicinity of compact HII regions with the Effelsberg 100 m telescope. This paper presents the first results, namely positions and spectra for 82 H_2O sources, 32 of which are new discoveries. One of the sources 30.9+0.1, is probably associated with a late-type star, but

Max-Planck-Gesellschaft zur Förderung der Wissenschaften e.V.
M.P.I. f. Radioastronomie, Bonn
Sonderdruck Nr. 218, Ser. A

we believe that most of the rest are probably newly-formed stars. The sources lie between $\ell = 0.5°$ and 232°, and are mostly confined to within 1° of the galactic equator. We searched toward radio continuum sources (Altenhoff *et al.* 1978, Israel 1976c) and OH sources (Caswell and Robinson 1974, Robinson *et al.* 1970, Evans *et al.* 1976, Knowles *et al.* 1976). For most of the 50 previously known water vapor sources in our list we have considerably improved their positions and spectral information.

2. OBSERVATIONS

The observations were made during October 1976–February 1977 with the same equipment, sensitivity and observing technique as described in our earlier paper on the Orion Nebula (Genzel and Downes 1977, hereafter GD77). The beamwidth of the 100 m telescope at 22 GHz is 40″. After having found a source, we mapped it with half-beamwidth spacing, with a minimum grid size of 4×4 points. The integration time was one to three minutes, and the rms sensitivity was about 0.5 K in nearly all cases. With a single map the positional accuracy was $\pm 4''$ to $\pm 10''$, depending on the source intensity. For some sources, we achieved higher accuracy by averaging several maps.

The sources are listed in table 1, and almost all spectra are shown in figures 1 to 6. The spectra are arranged in the same order as in table 1, by right ascension of the source. In the figures, an antenna temperature of 1 K corresponds on the average to 2.6 Jy. For sources with $\ell < 20°$, 1 K corresponds to about 3.2 Jy, because of atmospheric extinction.

Most of the column headings in table 1 are self-explanatory:

Column 2: Gives the familiar source name. In cases where we found new sources near previously known ones, we have simply added (1), (2), etc. Sources which might be physically associated, such as the two sources in W3–IRS5 and in Sgr B2 N are further indicated by (a), (b).

Column 5: Lists the positional error ($\pm$) in both coordinates. For a few sources, positions have been measured to better than $\pm 2''$ with the Hat Creek interferometer (Hills *et al.* 1972, Baudry *et al.* 1974, Forster *et al.* 1977). For these sources we have listed the Hat Creek positions.

Column 6: Lists the approximate velocity centroid of the H_2O spectrum. For the exact line velocities, refer to the spectra in figures 1 to 6.

Column 7: Gives the separation, $\Delta V/2$, of the major line groups from the velocity centroid. This "low velocity emission" is discussed in detail in the subsequent section on source statistics.

Column 8: Describes the appearance of the spectrum in fall 76–winter 77. S = single line or one prominent single group; D = well-separated double lines or groups of lines; T = triple lines or triple groups of lines; SC = source complex = a rich spectrum, possibly composed of individual doubles or triples, for which we suspect that the H_2O "source" is in reality a complex of several stellar sources.

Column 9: Contains a "Y" (= yes) if the H_2O emission is correlated in position and velocity with a type I OH source.

Column 10: Gives the half extent, $\Delta V^H/2$, of the "high velocity features" toward the negative (indicated by "−") or positive ("+") velocity side of the spectrum. See the definition of "high velocity features" in the section on source statistics.

Column 11: Gives the kinematic distance. For sources within the solar circle, we list distances only when the distance ambiguity can be resolved by HI absorption lines (Radhakrishnan *et al.* 1972, Caswell *et al.* 1975), or when the associated HII region is optically visible (Georgelin and Georgelin 1976).

Columns 14 and 15: List references by authors' initials and year of publication. For some references with many authors, we only use the initials of the first two authors. For example, CR76 is Cato *et al.* (1976), GK76 is Goss *et al.* (1976).

3. COMMENTS ON SELECTED SOURCES

3.1. The W3 Region

W3(1) is a new H_2O source 30″ north of the radio continuum peaks W3C and D (*cf.* Harris and Wynn-Williams 1976).

W3(2a and b) is referred to as "W3 continuum" in the previous literature. The maser emission comes from IRS 5, which at 10μ has the deepest silicate absorption feature known (Willner 1977). IRS 5 is a double source in both the infrared (see Wynn-Williams 1976) and the H_2O emission (Forster *et al.* 1977). We list the Hat Creek interferometer positions for the two sources in IRS 5 in table 1.

W3(3) is another new H_2O source, located 68″ east of the radio continuum peak no. 7 on the map by Sullivan and Downes (1973). It has a double line spectrum with a wide separation (figure 1).

W3OH/H_2O is 7″ east of the OH and radio continuum source (Hills *et al.* 1972, Mader *et al.* 1975, Forster *et al.* 1977).

None of the H_2O sources coincides with the newly-found O stars in the W3 region (Ogura and Ishida 1976).

T Tauri

Knapp and Morris (1976) suggested that the H_2O maser was displaced by ~0.9′ from the position of the star. The Effelsberg data indicate that the emission is coming from T Tauri itself. Because of the weakness of the emission in the fall of 1976, the positional uncertainty is still large (±10″).

3.2. The Mon R2 Region

Our new observations resolve the H_2O emission into two single-line sources. Figure 7 shows their positions relative to the 10μ contours (Beckwith *et al.* 1976). $H_2O(1)$, with $V_{LSR}=11.2$ km s^{-1}, is west of the infrared cluster. $H_2O(2)$, at 11.8 km s^{-1}, coincides to within the errors with IRS3, the source with the strongest silicate absorption in Mon R2. One feature of the 1667 MHz OH maser emission has the same velocity as $H_2O(2)$, and may thus also come from IRS 3. The visible members of the stellar association (Herbst and Racine 1976) are mostly B stars, and the luminosities of the infrared cluster and the radio compact HII region suggest that these stars are also of type B. From the Mon R2 data, the H_2O masers associated with B stars seem to be about 500 times less luminous than, say, the Orion H_2O masers.

3.3 The Sgr B2 Region

We have discussed Sgr B2 elsewhere (Genzel *et al.* 1976). Table 1 gives our improved positional data.

Sgr B2 N has a complex H_2O spectrum, which may mean that the emission comes from a number of spatially distinct sources as in W49N. It is not clear whether the features at $V_{LSR}=90$ to 105 km s^{-1} (Sgr B2 Na) come from a separate H_2O source, or if they are "high velocity" fragments ejected from the main source, 4″ away.

Sgr B2M. Our new data show that the features at −24 to −28 km s^{-1} have the same position as the positive velocity group (figure 2). The source may therefore have a shell-type spectrum, with 100 km s^{-1} separation between the red and blue shifted features.

Sgr B2 S is slightly resolved with our 40″ beam, and may thus be a complex of several spatially separated H_2O sources.

H_2O 0.55–0.85. Kaufmann *et al.* (1976) and Knapp and Morris (1976) found features between −8 and 30 km s^{-1}, whereas the new Effelsberg data (figure 2) show that the spectrum in fact extends over a range of 120 km s^{-1}. All of the features in the spectrum come from the same position, to within ±2″. The velocity centroid of the H_2O spectrum, 45 km s^{-1}, differs considerably from the recombination-line velocity, 13 km s^{-1}, of the nearby HII region, G0.55–0.85 (Gardner and Whiteoak 1975, Pauls and Mezger 1975).

3.4. The W28 Region

W28 A2. In fall–winter 1976–77, we observed two sources which are separated by 18″ in Dec.

W28 A2(1) has a velocity centroid at $V_{LSR} = +14$ km s^{-1} and "high-velocity features" at V_{LSR} + 71 to 86 km s^{-1} and at $V_{LSR} = -61$ km s^{-1}. The latter feature is not shown in the spectrum of figure 2. To within the uncertainty of ±15″ in the OH position, H_2O(1) coincides with the OH emission at 1667 MHz (Hardebeck 1972).

W28 A2(2) appears to have a double-line spectrum, the features of which are blended with those of W28 A2(1) in figure 2.

During our observing period, we could not find the western H_2O source reported by Cato *et al.* (1976).

3.5. The M17 Region

Table 1 contains three sources in M17. We resolve H_2O (II) of Lada *et al.* (1976) into two sources, which we call M17(2) and (3). M17 appears to be similar in some respects to the Orion region. There is a cluster of hot stars which have ejected their shells and are no longer in the H_2O–emitting phase. These stars are barely visible in photographs at 9000 Å (Beetz *et al.* 1976). Some of the stars in this cluster ionize the compact radio continuum HII regions, and heat the dust which is seen as the extended infrared source.

The H_2O sources are probably in separate molecular clouds or cloud fragments of dimensions 10^{17} to 10^{18} cm, in much the same manner as the Kleinmann-Low Nebula in Orion is distinct from the fully-developed Trapezium cluster. The situation is sketched in figure 8. The diagonal dashed line represents the sharp transition zone between one of the molecular clouds, as seen in CO emission, and the HII region (Lada 1976).

H_2O 30.9+0.1. This is an extremely interesting source, probably a late-type star. To within the errors, the H_2O source coincides with an OH source which has the shell-type spectrum at 1612 MHz typical of Mira variables. The OH lines at 1612 and 1667 MHz are separated by seven km s^{-1} from a velocity centroid at 34 km s^{-1}.

The new result is that the H_2O lines (figure 4) are also symmetrically disposed about 35 km s^{-1}, but with a separation of ±90 km s^{-1}! This separation of 180 km s^{-1} is the largest yet observed in any symmetrical shell-type maser star in the radio range.

3.6. The W51 Region

H_2O 49.4–0.3 (W51 West) has a triple-peaked spectrum, and is apparently coincident with the radio continuum source G49.4–0.3, component "b" of Martin (1972). There is marginal evidence that the main features come from positions separated by a few arcsec.

W51 N is highly variable and has an interesting "triple" structure in its low-velocity emission, with an unusually large separation of ±33 km s^{-1} for the outer groups of the "triple". The source also has relatively strong "high velocity features" over a total range of 190 km s^{-1}. To within the errors (figure 9) the source coincides with the IR/radio continuum source 49.5–0.4, component "d" of Martin (1972). The infrared source has a deep silicate absorption at 10μ (Dyck and Simon 1977), which may occur in the same circumstellar shell as the H_2O emission.

W51 Main has a spectrum of the "Orion" type, with symmetric low velocity emission and weak high velocity features over a range of 140 km s^{-1}. In contrast to the 1665 MHz OH, the velocities of the 6035 MHz lines of excited OH are the same as those of the H_2O (Rickard *et al.* 1975). The intensity variations of this source are discussed in a later section.

W51 South is a new H_2O source with an apparent velocity centroid of $V_{LSR} = +7$ km s^{-1}, an unusual velocity for W51. The source could have equally strong emission, however, at $\sim +60$ km s^{-1}, which would be totally dominated in our mapping by the strong lines from W51 Main. Mader *et al.* (1977) observed OH emission at

58.4 km s^{-1}, and measured its displacement from the H_2O emission in W51 Main. Their OH position is only 2.7″ north of our W51S position, indicating that the OH at this velocity may come from W51S.

The feature at -9.8 km s^{-1} shown in figure 9 appeared only in our map of February 1977. It may be a fifth H_2O source in W51.

3.7. The W75 Region

W75N–OH has a triple-peaked spectrum (figure 6), and there may be an inverse correlation ("mode switching") in the intensity variations of the triple features. Figure 10 shows that to within the errors, the H_2O source coincides with the 1665 MHz OH position (Hardebeck 1972) and with the 53μ peak (Harvey *et al.* 1977). It is displaced 5″ from the radio continuum point source (Habing *et al.* 1974, Harris 1974, Matthews *et al.* 1977), but this displacement is just barely significant. The blue-shifted H_2O velocities are similar to those of the OH features in the interferometer map of Harvey *et al.* (1974).

W75S(1) had a spectrum consisting of a single line at -2.9 km s^{-1} in 1977, January–February, and was not detectable in 1976, October–December.

DR21. We have discovered an H_2O maser at the position of the continuum source DR21–S. The spectrum consists of a single line at a velocity of -6.0 km s^{-1}. Figure 11 shows the position of the H_2O maser relative to the continuum components mapped by Harris (1973).

W75S(2) (also called W75S–OH in the literature) is resolved by our measurements into two complexes, possibly a double star, separated by ~0.1 pc. Figure 12 shows our averaged map, together with the positions of the 1665 MHz OH emission (Raimond and Eliasson 1969) and the infrared peaks at 20μ (Wynn-Williams *et al.* 1974a) and 53μ (Harvey *et al.* 1977). No compact radio continuum source has been found in this region to a limit of 15 mJy at 5 GHz (Harris 1974). The two H_2O sources are both highly variable and ~20% linearly polarized (Bologna *et al.* 1975). Both sources, which we call W75S(2a) and (2b), have double-peaked spectra, and may thus be shell-type sources. From the velocity coincidences and the near overlap in the positional error bars, we think that the H_2O sources and the OH and IR sources are probably the same objects.

W75S(3) is a new source of the "shell type", with two groups of lines separated by ± 17 km s^{-1} from a velocity centroid at $V_{LSR} = -20$ km s^{-1}.

3.8. The NGC 7538 Region

NGC 7538–IRS 1. Figure 13 shows our improved map of this source (*cf.* Genzel and Downes 1976). The flux of the strongest line at -61 km s^{-1} increased from 200 Jy in May 1976 to a maximum of about 700 Jy in October–December, 1976. This line dominated the spectrum, and any possible shell symmetry is thus difficult to recognize. We have also mapped the "high velocity features" in the range -88 to -42 km s^{-1} with better sensitivity than in our earlier paper. The feature at -84.6 km s^{-1} definitely seems to lie 7″ west of the main line. It may thus come from high velocity material ejected from the main source, IRS 1. The source NGC 7538–IRS 1 and ON 1 are the only definite cases so far where the H_2O emission is coincident on a scale $< 10^{16.5}$ cm with a "super"-compact HII region. The radio continuum source in NGC 7538–IRS 1 has an angular diameter of $\leq 0.7'' \times 1.2''$ and an emission measure $> 10^8$ cm^{-6} pc (Harris and Scott 1976).

4. STATISTICAL ANALYSIS

4.1. Low and High Velocity Emission

As we have explained in our paper on Orion (Genzel and Downes 1977), there are two different types of H_2O emission:

i) The strong, low velocity emission usually occurs in a narrow range in velocity (< 15 km s^{-1}), often with symmetrical arrangement of lines or line groups about a central velocity. It is confined to spatial complexes ~10^{16} cm in size.

ii) The high velocity features are highly variable and weak, with 0.1 to 10% the intensity of the low velocity emission, and with velocities displaced by more than 20 km s^{-1} from the low velocity centroid. The lines come from points scattered over an extent of $10^{16.5}$ to $10^{17.5}$ cm around the low velocity complexes. About 14 sources in our list have these weak, high velocity features. To our knowledge, direct measurements showing the extent of the high velocity features exist only for two of the sources, W49N and Orion KL (Knowles *et al.* 1974, Walker *et al.* 1977, Genzel and Downes 1977). Two further cases where high velocity features may be coming from points significantly displaced from the low velocity emission are Sgr B2 N and NGC 7538–IRS 1 (see the comments on the sources, this paper).

Since 14 of the 30 strongest sources in our list have high velocity features, we suspect that nearly all H_2O sources have high velocity features during most of their evolution, and that their detection is largely a question of instrumental sensitivity.

4.2. Low velocity Emission: Symmetries

Many of the spectra in figures 1 to 6 can be classified by the following types of low velocity emission (*cf.* Knowles 1976). Typical representatives are listed in parenthesis.

i) The spectrum consists of only a single (S) line (W33B, NGC 2024, and the two sources in Mon R2.)

ii) The spectrum is double (D) peaked, which we interpret as arising in a circumstellar shell. Each of the "shell" peaks may consist of a single line or of a group of lines (W3(3), M17(1), S235, Sgr B2 M). The individual lines in a group are usually separated by 1.5 to 3 km s^{-1}. As we pointed out in our paper on Orion (Genzel and Downes 1977), this is not hyperfine splitting. It is probably a fundamental kinematic property of the dust shells.

iii) A further well-defined group of sources (*e.g.* W51 Main, 29.9–0.0, S255, Orion KL) have in addition to the double-peaked, "shell" emission, further emission near the velocity centroid of the outer two peaks. We call this type of spectrum "triple" (T).

More than 65% of all H_2O sources fit in these categories. Apart from weak sources near our detection limit, the remainder of the sample probably consists of sources like W49N which are a spatial complex of sources with many overlapping lines from different, unresolved centers. "Single line" sources probably do not really exist, but may belong to the "double" or "triple" class, the other components being below our limit of detection.

Figure 14 shows the number of sources as a function of half of the range $\Delta V/2$, of the low velocity emission. This parameter corresponds to the expansion or contraction velocity of the circumstellar shell around a massive young star (Reid *et al.* 1977, Olnon 1977, Genzel and Downes 1977). The tail of the distribution in figure 14 contains an interesting group of sources with a large range in their "low velocity" emission. ($\Delta V/2 \geq 20$ km s^{-1}). Except for Sgr B2 N, 30.8–0.1 and W49N, all of these sources have "double" line groups or symmetrical "triple" groups of lines, and should probably be regarded as individual shell sources, rather than sources with "high velocity features". There is no significant difference in the velocity range of double and triple-peaked spectra.

Since H_2O sources are variable on the order of months, any detailed interpretation of symmetry in a single spectrum is open to question. We think that the examples of Orion and W51, however, demonstrate the persistence of the main "shell pattern" in the spectra over a time scale of many years.

5. H_2O LUMINOSITY FUNCTION

Figure 15 shows the luminosity function for the H_2O sources observed in fall–winter 1976–77. The H_2O luminosity is an approximate integral over all lines observed, and we assumed that the masers radiate isotropically over 4π steradians. The uppermost distribution is the luminosity function for all H_2O sources in our list with known distances. The median luminosity is 3 10^{29} erg s$^{-1} \sim 10^{-4}$ $L_\odot$, with a standard deviation of a factor of 10. This result agrees well with the luminosity function given by Johnston *et al.* (1973), indicating that the intensity variations of H_2O sources have little effect on the overall statistics.

The lower histograms in figure 15 are the distributions for the different classes of H_2O spectra. The figure shows the following results:

a) Sources which apparently have only one line ("singles") are on the average at least ten times weaker than the other sources, and tend to be within a few kpc of the sun. They may represent a separate population of H_2O sources, possibly associated with less massive stars (for example, T Tauri and the two H_2O sources in Mon R2).

b) There is some evidence that sources with triple-peaked spectra are two to four times more luminous than sources with double-peaked spectra.

c) Sources with complex spectra are more luminous than those in the other classes, which may be further evidence that they are unresolved clusters of individual H_2O sources, like W49N.

6. INTENSITY VARIATIONS

We discuss here only a new type of correlated intensity variation which seems to occur in the low velocity emission of symmetric shell sources (W51 Main, W75 N–OH, W75S(3), 10.5+0.0). For studies of other types of H_2O variability see Buhl *et al.* (1969), Sullivan (1973), Gammon (1975).

The new type of variation is as follows: Lines which are nearby in velocity ($\Delta V \sim 2$ km s^{-1}) vary inversely. That is, they interchange their relative strength over a period of three to ten months, whereas the sum of their line intensities remains nearly constant, or is at least much less variable than the individual lines themselves.

Figure 16 shows these relative intensity variations in the case of the three main line groups in the low velocity emission of W51 Main. The low velocity emission of W51 Main forms a typical triple-peaked spectrum. Each of the three groups of the triple has sub-lines. Figure 16 shows the variation of these sub-lines as well as their sums over an interval of three years. To reduce calibration and pointing errors, we divided the intensities by the sum of all six sub-lines considered. The changeover in intensity is often dramatic; note the logarithmic scale in figure 16. Although the narrow velocity separation is comparable with the hyperfine splitting of H_2O, in no case do we find a consistent agreement of the hyperfine intervals and the observed separations. Furthermore, in Orion KL (Genzel and Downes 1977), the maser lines of Si0 show the same splitting as H_2O. We therefore think that the splitting is determined by the kinematics of the circumstellar shells.

The effect probably must be interpreted in terms of a saturated travelling-wave maser with several modes, which are determined by the kinematics of the circumstellar matter. An appropriate designation for this behavior might be "mode switching" or "mode drifting".

7. RELATION OF H_2O MASERS TO IR AND OH SOURCES AND TO COMPACT HII REGIONS

Figure 17 compares the positional displacements of H_2O sources and compact HII regions, infrared sources and class I OH sources at 1665 MHz. We used only interferometer positions for the OH and radio continuum sources. Some of the OH positions however, have large uncertainties. Figure 17 shows the following results:

a) Non-coincidence of H_2O and compact HII regions mapped to date

Most of our H_2O sources are in the vicinity of compact HII regions (projected separation ≤ 0.3 pc), but only 10 to 20% of the sources with reliable positions coincide to better than 0.1 pc. This means that in a statistical sense, the compact HII regions mapped to date are not coincident with H_2O sources. (There may of course be a class of super compact HII regions like NGC 7538–IRS 1 which do coincide with H_2O masers, but which are mostly below current limits of detection in the radio continuum).

b) Two kinds of IR sources

Our sample of IR sources contains only 18 objects, which can be equally divided into two types (see *e.g.* Wynn-Williams and Becklin 1974). The first type does not coincide with the H_2O, and is emitted by

heated dust in and around the compact HII regions, with emission predominantly in the near infrared (Wynn-Williams *et al.* 1972, see also the discussion by Krügel and Mezger 1975, and Mezger and Smith 1977).

The second type of IR emission comes from cooler dust in the compressed shells around young stars, and is often characterized by silicate absorption at 10 microns. The projected linear separation of the H_2O sources and this second type of IR source is <0.1 pc. We think that the H_2O emission and this second type of IR radiation originate in the same circumstellar shell.

c) OH lines from the circumstellar shell

Although it is clear from figure 17 and from interferometric results (Hills *et al.* 1972, Mader *et al.* 1975, Forster *et al.* 1977) that many OH sources are displaced from the H_2O masers, there is probably a second class of OH emission which comes from the same position as the H_2O. This can be better shown by a comparison of the velocities of the OH and H_2O maser lines.

Figures 18 and 19 show the velocity correlation between H_2O and OH, and, for comparison, formaldehyde. In the uppermost diagram of figure 18 we have plotted the number of sources per velocity interval as a function of the difference between V_{H_2O}, the H_2O velocity centroid, and V_{H_2CO}, that of the formaldehyde line at 4.8 GHz. The data show that the velocity of the newly-formed, massive stars, represented by V_{H_2O}, and that of the molecular clouds are related. The ± 8 km s^{-1} dispersion of the symmetric distribution can be interpreted as the small-scale turbulent velocity of the interstellar gas (*cf.* von Hoerner 1975). The lowermost part of figure 18 is the same distribution, with V_{H_2CO} replaced by V_{OH}, the centroid of the OH emission at 1665 MHz. The apparent resemblance of the plots for OH and H_2CO would lead to the erroneous conclusion that the OH and H_2O are only spatially correlated on a scale of $\sim 10^{18}$ cm.

Let us, however, limit the sample to those H_2O sources with single lines or with lines symmetrically displaced by an amount $\Delta V/2$ from the H_2O velocity centroid. We then form the difference $V_{H_2O} - V_{OH} \pm \Delta V/2$, that is, we compare the OH with the actual velocities of the H_2O lines. The resulting distribution (figure 18, middle part) has a sharp peak for $|V_{H_2O} - V_{OH} \pm \Delta V/2| \leq 1$ km s^{-1}. This means that some of the OH lines are related to the H_2O sources on a much smaller linear scale ($\leq 10^{16}$ cm), with the OH emission coming from the same part of the circumstellar shell as the H_2O. These OH/H_2O sources are marked by a (Y) in column 9 of table 1.

Figure 19 proves this in an unbiased manner. The sample is the same as in figure 18, middle part. We have plotted the distribution for $V_{H_2O} - V_{OH} + \Delta V/2$ and for comparison, for $V_{H_2O} - V_{H_2CO} + \Delta V/2$. For the formaldehyde, the result is a net shift of the smooth distribution of figure 18 in the positive direction.

The same histogram for the OH sources, however, shows that some of the OH velocities are the same as the H_2O velocities. The same result appears if one uniformly plots $V_{H_2O} - V_{OH} - \Delta V/2$. The histograms thus indicate that some of the OH lines come from the red- or blue-shifted parts of the expanding circumstellar shells.

8. POSSIBLE EVOLUTIONARY SCHEME

Table 2 sketches how the different types of H_2O sources might be related to stages in the evolution of a massive OB star (Wynn-Williams and Becklin 1974, Israel 1976c, Mezger and Smith 1977, Yorke and Krügel 1977, Cochran and Ostriker 1977).

Our list includes ~ 80 sources which are probably young OB stars with masses $>5\ M_\odot$. The total number of such stars which emit H_2O lines above our limit of detection is probably ≥ 200. If we assume the Salpeter luminosity function and the current star formation estimates of $\sim 0.6\ M_\odot$/year for stars larger than 5 $M_\odot$ (Smith *et al.* 1977), we derive a lifetime of the H_2O phase of $\geq 10^4$ years, which is roughly consistent with the outline presented in table 2.

ACKNOWLEDGEMENTS

We are especially grateful to Sharon Beck for help with the observations and data reduction. We thank J. Lequeux and D. and C. Cesarsky for pointing out to us the source W3(3). P.G. Mezger, J.L. Caswell and A. Winnberg gave useful comments, and O. Genzel-Boroviczény and J. Bieging also helped with some of the observing.

REFERENCES

Allen, D.A.: 1972a, *Astrophys. J. Letters* **172**, L55.
Allen, D.A.: 1972b, *Astrophys. Letters* **12**, 231.
Altenhoff, W.J., Downes, D., Pauls, T.A. and Schraml, J.: 1978, in prep.
Baudry, A., Forster, J.R. and Welch, W.J.: 1974, *Astron. Astrophys.* **36**, 217.
Beetz, M., Elsässer, H., Poulakos, C. and Weinberger, R.: 1976, *Astron. Astrophys.* **50**, 41.
Beckwith, S., Evans, N.J., Becklin, E.E. and Neugebauer, G.: 1976, *Astrophys. J.* **208**, 390.
Bieging, J.H.: 1976, *Astron. Astrophys.* **51**, 289.
Bologna, J.M., Johnston, K.J., Knowles, S.H., Mango, S.A. and Sloanaker, R.M.: 1975, *Astrophys. J.* **199**, 86.
Buhl, D., Snyder, L.E., Schwartz, P.R. and Barrett, A.H.: 1969, *Astrophys. J. Letters* **158**, L97.
Caswell, J.L., Batchelor, R.A., Haynes, R.F. and Huchtmeier, W.K.: 1974, *Australian J. Phys.* **27**, 417.
Caswell, J.L. and Robinson, B.J.: 1974, *Australian J. Phys.* **27**, 629.
Caswell, J.L., Murray, J.D., Roger, R.S., Cole, D.J. and Cooke, D.J.: 1975, *Astron. Astrophys.* **45**, 239.
Caswell, J.L., Batchelor, R.A.,, Goss, W.M., Haynes, R.F., Knowles, S.H., Wellington, K.J., Yabsley, D.E. and Balister, M.: 1976, *Proc. Astron. Soc. Australia* **3**, 61.
Cato, B.T., Rönnäng, B.O., Rydbeck, O.E.H., Lewin, P.T., Yngvesson, K.S., Cardiasmenos, A.G. and Shanley, J.F.: 1976, *Astrophys. J.* **208**, 87.
Cochran, W.D. and Ostriker, J.P.: 1977, *Astrophys. J.* **211**, 392.
Dickinson, D.F.: 1976, *Astrophys. J. Suppl.* **30**, 259.
Downes, D., Winnberg, A., Goss, W.M. and Johansson, L.E.B.: 1975, *Astron. Astrophys.* **44**, 243.
Dyck, H.M. and Simon, T.: 1977, *Astrophys. J.* **211**, 421.
Elldér, J., Rönnäng, B. and Winnberg, A.: 1969, *Nature* **222**, 67.
Evans, N.J., Crutcher, R.M. and Wilson, W.J.: 1976, *Astrophys. J.* **206**, 440.
Forster, J.R., Welch, W.J. and Wright, M.C.H.: 1977, *Astrophys. J.*, in press.
Gammon, R.H.: 1975, *Astron. Astrophys.* **50**, 71.
Gardner, F.F., Whiteoak, J.B.: 1975, *Monthly Notices Roy. Astron. Soc.* **171**, 29P.
Genzel, R. and Downes, D.: 1976, *Nature* **262**, 564.
Genzel, R., Downes, D. and Bieging, J.: 1976, *Monthly Notices Roy. Astron. Soc.* **177**, 101P.
Genzel, R. and Downes, D.: 1977, *Astron. Astrophys.*, in press.
Georgelin, Y.M. and Georgelin, Y.P.: 1976, *Astron. Astrophys.* **49**, 57.
Goss, W.M., Lockhart, I.A., Fomalont, E.B. and Hardebeck, E.G.: 1973, *Astrophys. J.* **183**, 843.
Goss, W.M., Knowles, S.H., Balister, M., Batchelor, R.A. and Wellington, K.J.: 1976, *Monthly Notices Roy. Astron. Soc.* **174**, 541.
Gruber, G.M. and de Jager, G.: 1976, *Astron. Astrophys.* **50**, 313.
Habing, H.J., Goss, W.M., Matthews, H.E. and Winnberg, A.: 1974, *Astron. Astrophys.* **35**, 1.
Hardebeck, E.G.: 1972, *Astrophys. J.* **172**, 583.
Harris, S.: 1973, *Monthly Notices Roy. Astron. Soc.* **162**, 5P.
Harris, S.: 1974, *Monthly Notices Roy. Astron. Soc.* **166**, 29P.
Harris, S.: 1976a, *Monthly Notices Roy. Astron. Soc.* **174**, 1.
Harris, S.: 1976b, *Monthly Notices Roy. Astron. Soc.* **174**, 601.
Harris, S. and Wynn-Williams, C.G.: 1976, *Monthly Notices Roy. Astron. Soc.* **174**, 649.
Harris, S. and Scott, P.F.: 1976, *Monthly Notices Roy. Astron. Soc.* **175**, 371.
Harvey, P.J., Booth, R.S., Davies, R.D., Whillet, D.C.B. and McLaughlin, W.: 1974, *Monthly Notices Roy. Astron. Soc.* **169**, 545.
Harvey, P.M., Campbell, M.F. and Hoffmann, W.F.: 1977, *Astrophys. J.* **211**, 786.
Herbst, W. and Racine, R.: 1976, *Astron. J.* **81**, 840.
Hills, R., Janssen, M.A., Thornton, D.D. and Welch, W.J.: 1972, *Astrophys. J. Letters* **175**, L59.
Israel, F.P., Habing, H.J. and de Jong, T.: 1973, *Astron. Astrophys.* **27**, 143.
Israel, F.P.: 1976a, *Astron. Astrophys.* **48**, 193.
Israel, F.P.: 1976b, *Astron. Astrophys.* **52**, 175.
Israel, F.P.: 1976c, Ph. D. thesis, University of Leiden.
Israel, F.P.: 1977a, *Astron. Astrophys.* , in press.
Israel, F.P.: 1977b, *Astron. Astrophys.*, in press.
Johnston, K.J., Sloanaker, R.M. and Bologna, J.M.: 1973, *Astrophys. J.* **182**, 67.
Kaufmann, P.: 1976, *Nature* **260**, 306.
Kleinmann, D.E. and Wright, E.L.: 1973, *Astrophys. J. Letters* **185**, L131.
Knapp, G.R. and Brown, R.L.: 1976, *Astrophys. J.* **204**, 21.
Knapp, G.R. and Morris, M.: 1976, *Astrophys. J.* **206**, 713.
Knowles, S.H., Johnston, K.J., Moran, J.M., Burke, B.F., Lo, K.Y. and Papadopoulos, G.D.: 1974, *Astron. J.* **79**, 925.

Knowles, S.H.: 1976, *Proc. Astron. Soc. Australia* **3**, 55.
Knowles, S.H., Caswell, J.L. and Goss, W.M.: 1976, *Monthly Notices Roy. Astron. Soc.* **175**, 537.
Krügel, E. and Mezger, P.G.: 1975, *Astron. Astrophys.* **42**, 441.
Lada, C.J.: 1976, *Astrophys. J. Suppl.* **32**, 603.
Lada, C.J., Dickinson, D.F., Gottlieb, C.A. and Wright, E.L.: 1976, *Astrophys. J.* **207**, 113.
Lo, K.Y., Burke, B.F. and Haschick, A.D.: 1975, *Astrophys. J.* **202**, 81.
Low, F.J., Johnson, H.L., Kleinmann, D.E., Latham, A.S. and Geisel, S.L.: 1970, *Astrophys. J.* **160**, 531.
Mader, G.L., Johnston, K.J., Moran, J.M., Knowles, S.H., Mango, S.A., Schwartz, P.R. and Waltman, W.B.: 1975, *Astrophys. J. Letters* **200**, L111.
Mader, G.L., Johnston, K.J. and Moran, J.M.: 1977, *Astrophys. J.*, in press.
Martin, A.H.M.: 1972, *Monthly Roy. Astron. Soc.* **157**, 31.
Martin, A.H.M. and Downes, D.: 1972, *Astrophys. Letters* **11**, 219.
Martin, A.H.M.: 1973, *Monthly Notices Roy. Astron. Soc.* **163**, 141.
Matthews, H.E., Goss, W.M., Winnberg, A. and Habing, H.J.: 1973, *Astron. Astrophys.* **29**, 309.
Matthews, H.E., Goss, W.M., Winnberg, A. and Habing, H.J.: 1977, *Astron. Astrophys.*, in press.
Mezger, P.G. and Smith, L.F.: 1977, invited Review Paper held at *IAU Symposium 75,* Geneva, in press.
Moran, J.M., Papadopoulos, G.D., Burke, B.F., Lo, K.Y., Schwartz, P.R., Thacker, D.L., Johnston, K.J., Knowles, S.H., Reisz, A.C. and Shapiro, I.I.: 1973, *Astrophys. J.* **185**, 535.
Moran, J.M., Ball, J.A., Yen, J.L., Schwartz, P.R., Johnston, K.J. and Knowles, S.H.: 1977, *Astrophys. J.* **211**, 160.
Moran, J.M., Johnston, K.J., Spencer, J.H. and Schwartz, P.R.: 1977, *Astrophys. J.*, in press.
Morris, M. and Knapp, G.R.: 1976, *Astrophys. J.* **204**, 415.
Morris, M.: 1976, *Astrophys. J.* **210**, 100.
Ogura, K. and Ishida, K.: 1976, *Publ. Astron. Soc. Japan* **28**, 651.
Olnon, F.M.: 1977, Ph.D. thesis, University of Leiden.
Pauls, T. and Mezger, P.G.: 1975, *Astron. Astrophys.* **44**, 259.
Pipher, J.L., Grasdalen, G.L. and Soifer, B.T.: 1974, *Astrophys. J.* **193**, 283.
Pipher, J.L. and Soifer, B.T.: 1976, *Astron. Astrophys.* **46**, 153.
Radhakrishnan, V., Goss, W.M., Murray, J.D. and Brooks, J.W.: 1972, *Astrophys. J. Suppl.* **24**, 49.
Raimond, E. and Eliasson, B.: 1967, *Astrophys. J. Letters* **150**, L171.
Raimond, E. and Eliasson. B.: 1969, *Astrophys. J.* **155**, 817.
Reid, M.J., Muhleman, D.O., Moran, J.M., Johnston, K.J. and Schwartz, P.R.: 1977, *Astrophys. J.* **214**, 60.
Rickard, L.J., Zuckerman, B. and Palmer, P.: 1975, *Astrophys. J.* **200**, 6.
Rieke, G.H., Low, F.J. and Kleinmann, D.E.: 1973, *Astrophys. J. Letters* **186**, L7.
Robinson, B.J., Goss, W.M., Manchester, R.N.: 1970, *Australian J. Phys.* **23**, 363.
Smith, L.F., Biermann, P. and Mezger, P.G.: 1977, *Astron. Astrophys.*, in press.
Soifer, B.T. and Pipher, J.L.: 1975, *Astrophys. J.* **199**, 663.
Spencer, J.H. and Schwartz, P.R.: 1974, *Astrophys. J. Letters* **188**, L105.
Sullivan, W.T.: 1973, *Astrophys. J. Suppl.* **25**, 393.
Sullivan, W.T. and Downes, D.: 1973, *Astron. Astrophys.* **29**, 369.
Turner, B.E.: 1970, *Astrophys. Letters* **6**, 99.
Turner, B.E. and Rubin, R.H.: 1971, *Astrophys. J. Letters* **170**, L113.
Von Hoerner, S.: 1975, in T.L. Wilson and D. Downes (eds.), *HII Regions and Related Topics*, Springer, Berlin, p. 53.
Walker, R.C., Johnston, K.J., Burke, B.F. and Spencer, J.H.: 1977, *Astrophys. J. Letters* **211**, L135.
Webster, W.J., Altenhoff, W.J. and Wink, J.E.: 1971, *Astron. J.* **76**, 677.
Willner, S.P.: 1976, *Astrophys. J.* **206**, 728.
Willner, S.P.: 1977, *Astrophys. J.*, in press.
Wink, J.E., Altenhoff, W.J. and Webster, W.J.: 1975, *Astron. Astrophys.* **38**, 109.
Winnberg, A., Habing, H.J. and Goss, W.M.: 1973, *Nature* **243**, 78.
Wynn-Williams, C.G.: 1971, *Monthly Notices Roy. Astron. Soc.* **151**, 397.
Wynn-Williams, C.G., Becklin, E.E. and Neugebauer, G.: 1972, *Monthly Notices Roy. Astron. Soc.* **160**, 1.
Wynn-Williams, C.G. and Becklin, E.E.: 1974, *Publ. Astron. Soc. Pacific* **86**, 5.
Wynn-Williams, C.G., Becklin, E.E. and Neugebauer, G.: 1974a, *Astrophys. J.* **187**, 473.
Wynn-Williams, C.G., Werner, M.W. and Wilson, W.J.: 1974b, *Astrophys. J.* **187**, 41.
Wynn-Williams, C.G.: 1976, *Observatory* **96**, 6.
Yngvesson, K.S., Cardiasmenos, A.G., Shanley, J.F., Rydbeck, O.E.H. and Ellder, J.: 1975, *Astrophys. J.* **195**, 91.
Yorke, H.W. and Krügel, E.: 1977, *Astron. Astrophys.* **54**, 183.

R. Genzel
D. Downes

Max-Planck-Institut für Radioastronomie
Auf dem Hügel 69
D–5300 Bonn (Federal Republic of Germany)

Table 1 Parameters of H_2O Sources

(1)	(2)	(3)	(4)	(5)	(6)	(7)	(8)	(9)	(10)	(11)	(12)	(13)	(14)	(15)	(16)
Galactic Coord.	Source Name	R.A.(1950) (h m s)	Dec.(1950) (° ′ ″)	Error (″)	L.S.R. Vel. Centroid V_{H_2O} (km s^{-1})	Low Vel. Range $\Delta V/2$ (km s^{-1})	Low Vel. Type	Corr. with OH	High Vel. Range $\Delta V^H/2$ (km s^{-1})	Dist. (kpc)	1976/77 Flux of strongest line (Jy)	1976/77 Total H_2O Luminosity ($L_\odot$)	Previous H_2O Refs	Other References	Remarks
133.7+1.2	W3(1)	02 21 40.8	61 53 26	4	-49	-	S			3	15	$3\ 10^{-6}$		WW71	
"	W3(2a)	02 21 53.14	61 52 22.0	0.4	-41	3	-			3	550	$3\ 10^{-4}$	FWW77,HJTW72	HWW76,W77,WWBN72	see Text
"	W3(2b)	02 21 53.19	61 52 19.5	0.4	-35	2	D	?		3	550	$2\ 10^{-4}$	" "	" " "	
"	W3(3)	02 22 06.1	61 50 40	4	-54	15	D			3	110	$7\ 10^{-5}$			
133.9+1.1	W3(OH)	02 23 17.30	61 38 57.7	0.4	-48	5	-		±25	3	4000	$3\ 10^{-3}$	FWW77,S73,HJTW72	WWBN72,HS76,MJ75	consists of several sources?
176.2-20.9	T Tauri	04 19 04.2	19 25 05	10	+1.4	-	S			0.2	3	$3\ 10^{-9}$	KM76	SS74,LJKLG70	possibly two sources.
209.0-19.4	Orion KL-A	05 32 46.71	-05 24 28	2.5	+5.5	11	T	Y	±85	0.5	3000	$6\ 10^{-5}$	BFW74,MJS77,GD77	RLK73,RE67	For more detailed discussion see GD77
"	Orion KL-B	05 32 46.57	-05 24 31.5	3	+18	9	T		±85	0.5	4500	$4\ 10^{-5}$	" " "	" "	
173.7+2.7	S235	05 37 31.8	35 40 18	3	-30	30	D			2	13	$2\ 10^{-5}$	LBH75	I77a, H76b	
206.6-16.4	NGC2024	05 39 13.7	-01 57 30	6	+10		S			0.5	10	$6\ 10^{-8}$	JSB73		
213.7-12.6	MonR2(1)	06 05 17.0	-06 22 40	5	+11.2	-	S	Y		0.8	12	$2\ 10^{-7}$	MK76,KB76	BEBN76,DWGJ75	see Fig. 7
"	MonR2(2)	06 05 21.7	-06 22 35	5	+11.8	-	S	Y		0.8	8	$1\ 10^{-7}$	" "	" "	
192.6-0.0	S255	06 09 58.2	18 00 17	3	+17	10	T			1.3	300	$3\ 10^{-5}$	LBH75	I76b,PS76	H_2O coincides with IR source
196.5-1.7	S269	06 11 46.6	13 50 39	15	+19	2.5	T	Y		2	130	$1\ 10^{-5}$	LBH75	I76b, WWWW74,WWBN74	
203.3+2.1	NGC2264	06 38 25.2	09 32 12	3	+10	8	D			0.8	30	$8\ 10^{-7}$		A72a,b, H76b	H_2O is not Allen's IR source
231.8+4.2	0739-14	07 39 58.9	-14 35 38	7	+31	11	D	? ?		1.8	9	$1\ 10^{-6}$	MK76	WWBN74, WWWW74	
0.68-0.03	SgrB2N(a)	17 44 10.1	-28 21 13	4	+100	6	-			10	15	$2\ 10^{-4}$	GDB76,M76,GK76		Maybe high vel. feature of Sgr B2N(b)
"	SgrB2N(b)	17 44 10.2	-28 21 16.5	3	+50	22	SC		?	10	400	$1\ 10^{-2}$	" " "	MD72,	
0.67-0.03	SgrB2M	17 44 10.4	-28 22 00	4	+26	55	D	?	?	10	220	$5\ 10^{-3}$	" " "	MD72,B76	see Text
0.66-0.04	SgrB2S	17 44 10.6	-28 22 39	4	+63	7	SC	Y	?	10	1000	$4\ 10^{-3}$	" " "	B76,HCH77	
0.55-0.85	-	17 47 03.4	-28 53 39	5	+45	45	SC?			-	130	-	KM76	GW75	highly variable
5.9-0.4	W28A2(1)	17 57 26.8	-24 03 54	5	+14	6.5	D	?	±70	2.5?	45	$2\ 10^{-5}$	CR76,JSB73	H72	see Text
"	W28A2(2)	17 57 26.8	-24 04 12	5	+15	6.5	D	?		2.5?	45	$2\ 10^{-5}$	" "		
7.5+0.06	-	17 59 11.7	-22 28 13	7	-16	9 ?				-	10	-			
8.1+0.2	-	18 00 00.2	-21 48 29	7	+14		S			-	10	-			
10.5+0.0	W31(1)	18 05 40.5	-19 52 23	4	+64	6.5	T		±42	12	230	$4\ 10^{-3}$			
10.6-0.4	W31(2)	18 07 30.3	-19 56 38	4	-0.6	5	-	Y		6	490	$1\ 10^{-3}$	YC75,TR71,CB74	MGWH77,GLFH73	
12.2-0.1	(1)	18 09 43.5	-18 25 05.5	3	+7	30	D			6	300	$1\ 10^{-3}$			
12.2-0.1	(2)	18 09 48.5	-18 25 25	4	+25	4	D			-	60	-			
12.2-0.1	(3)	18 09 48.6	-18 25 17	6	+33	-	S			-	10	-			May be coincident with (2)
12.7-0.2	W33B	18 10 58.9	-18 02 39	4	+58	1.5	S	? Y		4.5	420	$3\ 10^{-4}$	JSB73	WWWW74	
13.2+0.04	-	18 11 11.5	-17 29 13	7	-1.6	3	-			-	30	-			H_2O differs 40 km s^{-1} from H_2CO
12.8-0.2	W33 CONT	18 11 18.3	-17 56 21	5	+20	22	D			4.5	25	$4\ 10^{-5}$		DS77	H_2O differs 26 km s^{-1} from H109α
13.9+0.3	-	18 11 41.5	-16 46 34	6	-21	12	T			-	100	-			H_2O differs 70 km s^{-1} from H_2CO
12.9-0.3	W33A	18 11 44.0	-17 53 08.5	5	+40	3.5	-	Y		4.5	30	$3\ 10^{-5}$		WWWW74, DS77	
14.6+0.0	-	18 14 08.1	-16 15 46	7	+31	2	-			4	24	$8\ 10^{-6}$			
15.0-0.7	M17(1)	18 17 30.0	-16 16 03	5	+4	8	D			2.5	50	$4\ 10^{-5}$	LDGW76,	KW73	see Fig. 8
"	M17(2)	18 17 30.3	-16 13 06	4	+19	2.5	D	Y		2.5	200	$5\ 10^{-5}$	LDGW76,CB74,JSB73,GK76		
"	M17(3)	18 17 31.1	-16 12 51	5	-27	2	D			2.5	30	$1\ 10^{-5}$			
19.6-0.2	-	18 24 50.1	-11 58 22	4	+36	7	T	Y		4	100	$3\ 10^{-4}$	TR71,CB76	MGWH77,GLFH73	
23.95+0.15	-	18 31 40.8	-07 57 17	7	+82	-	S			6	60	$5\ 10^{-5}$			
24.8+0.1	-	18 33 30.9	-07 14 27	20	+113	6	-			8	60	$4\ 10^{-4}$	TR71,CB76		Caswell (private comm.)
29.9-0.0	W43S	18 43 26.7	-02 42 40	4	+100	3.5	T			8.5	55	$3\ 10^{-4}$	KM76	SP75	Not coincident with IR source (SP75)
31.4+0.3	-	18 44 59	-01 16 07	7	+101	3.5	T			7.5	90	$3\ 10^{-4}$			
30.8-0.0	W43MAIN(1)	18 45 02.8	-02 00 45	5	+90	3	-			7.5	32	$2\ 10^{-4}$	CR76,YC75	PGS74	
"	W43MAIN(2)	18 45 02.8	-02 01 50	5	+51	2.7	D			-	8	-		PGS74	
30.9+0.1	W43OH1612	18 45 05.6	-01 48 39	4	+35	90	D			-	50	-		H72	Probably late-type star; see text
30.8-0.1	W43MAIN(3)	18 45 11.0	-01 57 57	4	+103	13	SC		±33 ?	8	100	$3\ 10^{-3}$	CB76		
30.8-0.2	W43MAIN(4)	18 45 33.1	-02 00 21	5	+97	1	D			7.5	13	$4\ 10^{-5}$	CR76,TR71		
31.4-0.3		18 46 57.5	-01 32 33	4	+89	4	-			7	16	$4\ 10^{-5}$			
32.8+0.2	(1)	18 47 57.3	-00 05 28	4	+6	2	D			16	15	$2\ 10^{-4}$			
"	(2)	18 47 57.4	-00 05 12	4	+23	-	S			16	10	$7\ 10^{-5}$			Another line at +34 km s^{-1} ?

Table 1 *(continued)*

(1)	(2)	(3)	(4)	(5)	(6)	(7)	(8)	(9)	(10)	(11)	(12)	(13)	(14)	(15)	(16)
Galactic Coord.	Source Name	R.A.(1950) (h m s)	Dec.(1950) (o ' ")	Error (")	L.S.R. Vel. Centroid V_{H_2O} (km s^{-1})	Low Vel. Range $\Delta V/2$ (km s^{-1})	Low Vel. Type	Corr. with OH	High Vel. Range $\Delta V^H/2$ (km s^{-1})	Dist. kpc (kpc)	1976/77 Flux of strongest Line (Jy)	1976/77 Total H_2O Luminosity L ($L_\odot$)	Previous H_2O Refs	Other References	Remarks
33.1-0.1	-	18 49 34	00 04 30	15	+75	1.5	D		-	-	23	-	JSB73		
33.9+0.1	-	18 50 16.3	00 51 45	15	+109	-	S		-	9	4	7 10^{-6}			
34.3+0.1	-	18 50 46.4	01 11 10	3	+58	13	-	?	±25	4	600	1 10^{-3}	YC75,CR76,CB76,TR71		
35.6-0.0	-	18 53 51.1	02 16 27	10	+57.5	6.5	T	Y		-	120	-	JSB73	KCG76,T70	
35.2-1.7	W48	18 59 12.8	01 09 13	10	+46	-	S			3	30	6 10^{-6}	TR71	DS77	
43.2+0.01	W49N	19 07 49.8	09 01 17	1	+10	40 ?	SC	?	±260	14	10^5	1.3	HJTW72,S73,BFW74,WJBS77	MJ75,RE69,HCH77,WAW75	
43.2-0.03	W49S	19 07 58.2	09 00 03	3.5	+10	6	D ?	?	?	14	550	3 10^{-2}	JSB73	HCH77,RE69,WAW75	
43.8-0.1	-	19 09 31.2	09 30 51	3	+41	2.8	T	?	±20	-	550	-		KCG76	
45.1+0.1	-	19 11 00.3	10 45 42	7	+63.5	2.8	T	Y		10	30	1 10^{-4}	LBH75	GLFH73,MGWH77	
45.44+0.1	-	19 11 56.8	11 03 33	10	+58	-	S	Y	-	9.5	5	1 10^{-5}	"	" "	
45.5+0.1	-	19 11 46	11 07 03	20	+45	-	S			-	1	-		GLFH73,MGWH77	marginal detection
48.6+0.0	-	19 18 13.1	13 49 43.5	4	+28	11	D ?	Y		12	35	4 10^{-4}	JSB73	CR74,T70	
49.4-0.3	W51W	19 20 53.3	14 20 47	4	+51.5	1.6	T			7	25	7 10^{-5}		M72	see Text
49.5-0.4	W51N	19 21 22.3	14 25 19	3	+33	33	T		$^{+80}_{+110}$	8 ?	360	1 10^{-2}	JSB73,CB76	M72,WWBN74,DS77	
"	W51S	19 21 26.3	14 24 30	5	+7 ?	12	-			8 ?	85	5 10^{-4}			see Figs.9, 16
"	W51MAIN	19 21 26.3	14 24 43	2	+63	8	T	?	$^{-80}_{+88}$	8	3000	1 10^{-2}	HJTW72,GK76,CB76,S73	WWWW74,DS77,WWBN74,M72	
70.3+1.6	K3-50	19 59 50.1	33 24 17	7	-19	7	-			9	3	2 10^{-5}		I76a	
"	ON-3	19 59 58.4	33 25 47	7	-19	2.2	D	Y		9	3	1 10^{-5}		WWWW74,I76a	
69.5-1.0	ON-1	20 08 09.8	31 22 44	3	+13	4	-	Y ?	$^{-80}_{+10}$	6 ?	200	7 10^{-4}	CR76,BFW74,S73	ERW69,WHG73,H72	H_2O may coincide with HII region
75.8+0.3	ON-2(1)	20 19 49.0	37 15 58	4	-8	3	D			5.5	85	1 10^{-4}	CR76	MGWH73	
"	ON-2(2)	20 19 51.6	37 17 00	3	-8	15	D		-40	5.5	350	1 10^{-3}	JSB73,CR76	ERW69,MGWH73,H76a	
81.9+0.8	W75N OH	20 36 50.45	42 27 01	2.5	+15	6	T	Y ?		3	300	1 10^{-4}	JSB73,CR76,YC75	WWBN74,HCH77,H72	see Fig. 10
81.7+0.6	W75S (1)	20 37 13.3	42 13 57	5	-3		S			3	15	3 10^{-6}			see Text
81.7+0.5	DR21	20 37 13.8	42 08 52	4	-6		S			3	30	6 10^{-6}		WWBN74,H73,DS77,HCH77	see Fig. 11
81.72+0.6	W75S (2a)	20 37 13.8	42 12 11	2.5	0	4.5	D	Y		3	300	9 10^{-5}	CR76,S73	RE69,WWBN74,HCH77	see Fig. 12
"	W75S (2b)	20 37 14.1	42 12 15	2.5	-4.3	4.2	D	Y		3	300	1 10^{-4}	" "	" " "	" " "
81.8+0.6	W75S (3)	20 37 16.7	42 15 15	4	-20	17	D			3	30	2 10^{-5}			
111.5-0.76	NGC7538S	23 11 36.3	61 10 29.5	2	-54.6	8	T	?		3.5	160	2 10^{-4}	JSB73,CR76,GD76,YC75	WWWW74	
111.5+0.78	NGC7538IR	23 11 36.5	61 11 49.5	2	-59 ?	1.5	D/T	Y	±22 ?	3.5	750	2 10^{-4}	GD76	WWWW74,M73,WWBN74,HS76	see Text + Fig. 13
111.3-0.67	S157	23 13 53.1	59 45 18	4	-46		S			3.5	30	8 10^{-6}		I77b	hyperfine splitting?

Table 2 Possible phases of H_2O emission in an evolutionary scheme for OB stars.

Evolutionary stage	Duration	dynamical effects	observational appearance	possible examples
1) Pure accretion phase	-	Infall of protostellar cloud at 2 to 5 km s^{-1} (scale 10^{18} cm).	Dense molecular cloud with low excitation molecules; CO self-absorption.	?
2) Stellar core forms and Star turns on	3 10^5 yr	Radiation pressure stops accretation flow at $\sim 10^{13}$ to 10^{14} cm; inner opaque cocoon forms; kinetic energy of accreting material heats the dust.	Far-IR source; OH maser, pumped by IR; H_2O emission with a narrow velocity range (small ΔV) appears toward the end of this phase.	W3IRS5 H_2O source near W3OH/IRS8
3) Cocoon begins to expand	2 10^4 yr	Radiation pressure increases further, due to nuclear burning of stellar core. Dust front/inner opaque cocoon expands from 10^{14} to 10^{16} cm at a velocity of 3 to 10 km s^{-1}. Possible outer cocoon at 10^{17} cm. The material outside the cocoon is still accreting.	Strong Far-IR source; H_2O "shell" type spectra ("triples") become well defined with a range of 3 to 10 km s^{-1}; OH maser lines occur at the same velocities as H_2O.	NGC7538S W75N-OH
4) Development of a super-compact HII region	-	Strong UV from star creates super-compact, dust-bounded HII region which expands at 1 - 10 km s^{-1}. A radiation-driven stellar wind begins to blow some fragments out of the dust shell. The outermost parts of the envelope may still be accreting.	Far-IR and near IR source; low velocity H_2O "shell" emission dominant, but some weak, high velocity features appear over a limited velocity range ($V^H \sim 30$ km s^{-1}). Supercompact HII region may be detectable in the radio continuum. Most of the UV photons are absorbed by the dust, however, so radio flux is not proportional to IR flux.	NGC7538-IRS1 ON1
5) Shell begins to fragment; stellar wind phase	10^4 yr	Strong stellar wind at 2 10^3 km s^{-1} blows out parts of shell from 10^{16} cm to 10^{17} cm; no significant accretion any more; compact HII region expands to 10^{16} cm but is still dust bounded.	Strong near and Far-IR emission; H_2O has strong low velocity emission as well as high velocity features over $\geq \pm 100$ km s^{-1}, possible SiO emission from low velocity shell(?); "hot" high velocity flow in CO and high excitation molecules, the compact HII region may be dectable in the radio continuum and the ratio of 20μ to 6 cm flux is relatively small.	W49N/H_2O W51Main Orion KL
6) Shell breaks up	-	The inner cocoon is unstable and breaks up; the expanding compact HII region is ionization bounded.	Strong near-IR emission; low-velocity H_2O emission looses its symmetrical pattern and its intensity decreases. The H_2O is highly variable, and the high velocity features are strong. The compact HII region is strong in the radio continuum.	W51N GO.55-0.85
7) Compact HII region expands	10^4 yr	HII region reaches 10^{17} cm (location of a possible outer cocoon?); H_2O molecules are broken up by UV, OH masers are pumped by UV.	Near IR radiation from the hot dust in the HII region. No H_2O maser is present. OH masers may be located at interface (10^{17} cm) with ionization front. The optically-thin radio continuum flux density is constant in time, while the turnover frequency is slowly decreasing. The radio flux is proportional to the near infrared flux.	Continuum and OH maser in W3OH/IRS8 (earlier phase); W3A/IRS1 (later phase)
8) HII region reaches edge of protostellar cloud (10^{18} cm)	3 10^4 yr	HII region becomes density bounded.	No H_2O or OH masers are present. The HII region is a near-IR, visible and UV source.	Trapezium Region in Orion

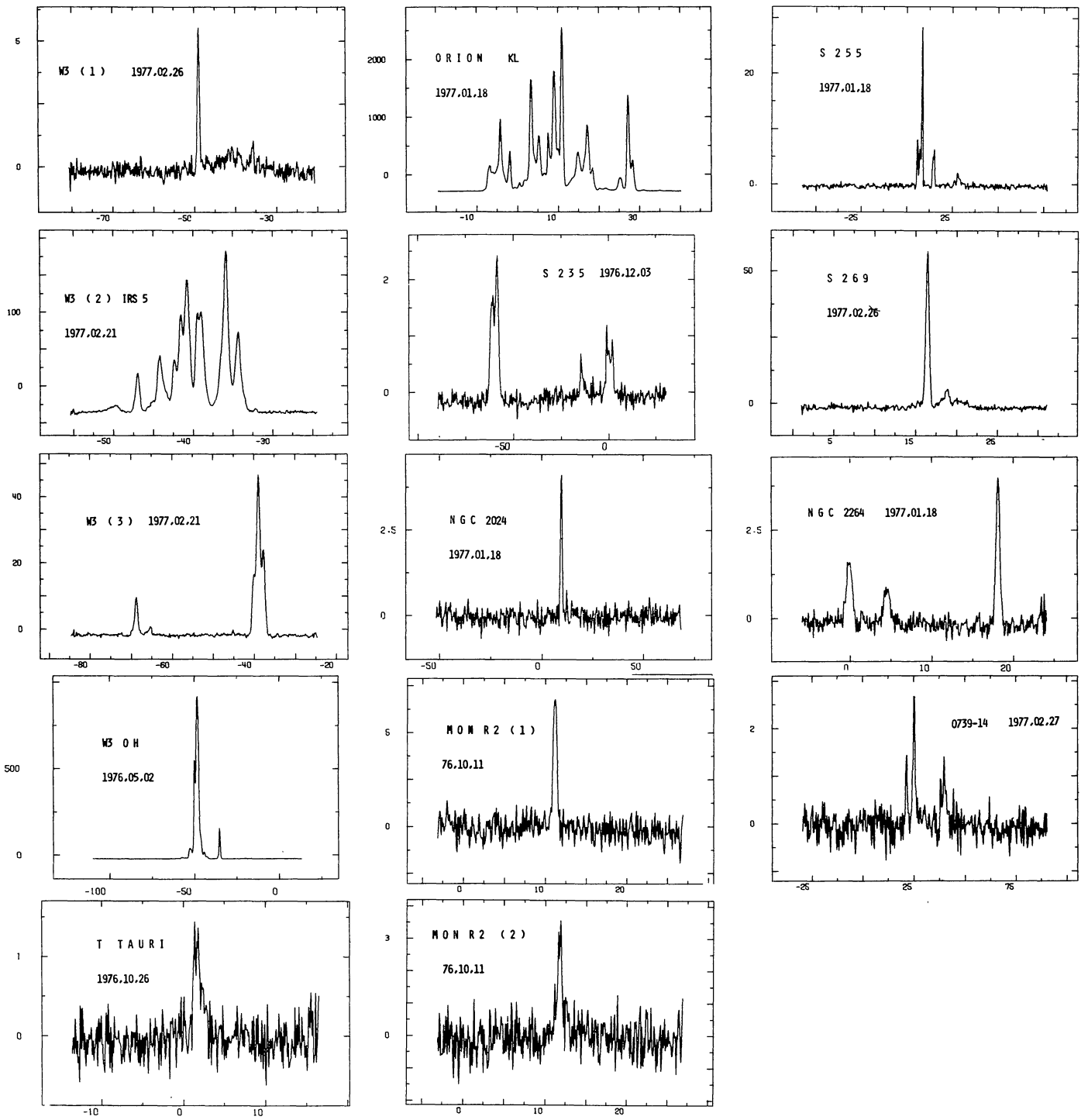

Figure 1

Figures 1–6 Spectra of the H_2O sources. Vertical axis is antenna temperature, in degrees K. Horizontal axis is velocity ($km\,s^{-1}$) relative to the local standard of rest. The date of observation (year, month, day) is given next to the source name.

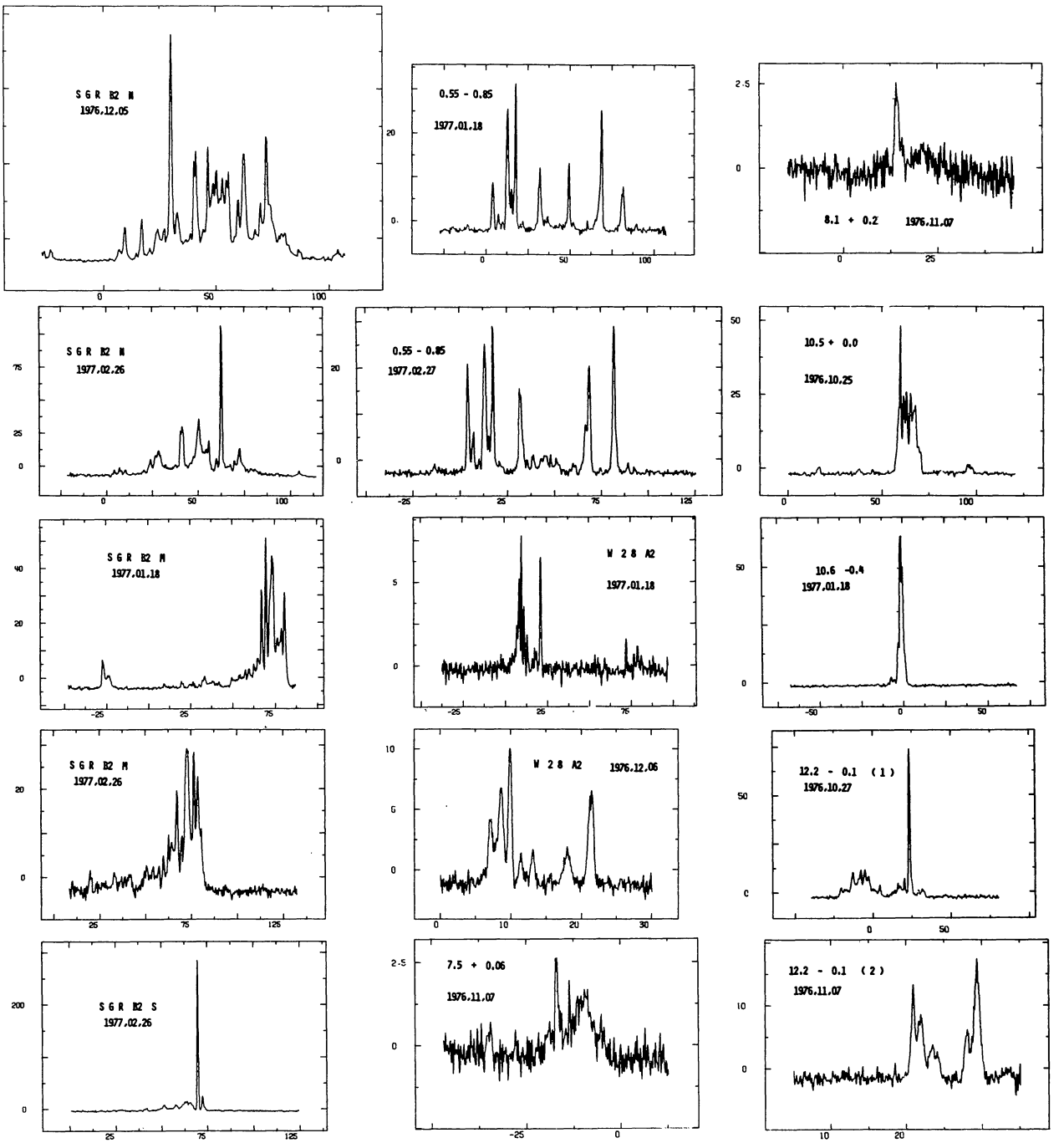

Figure 2

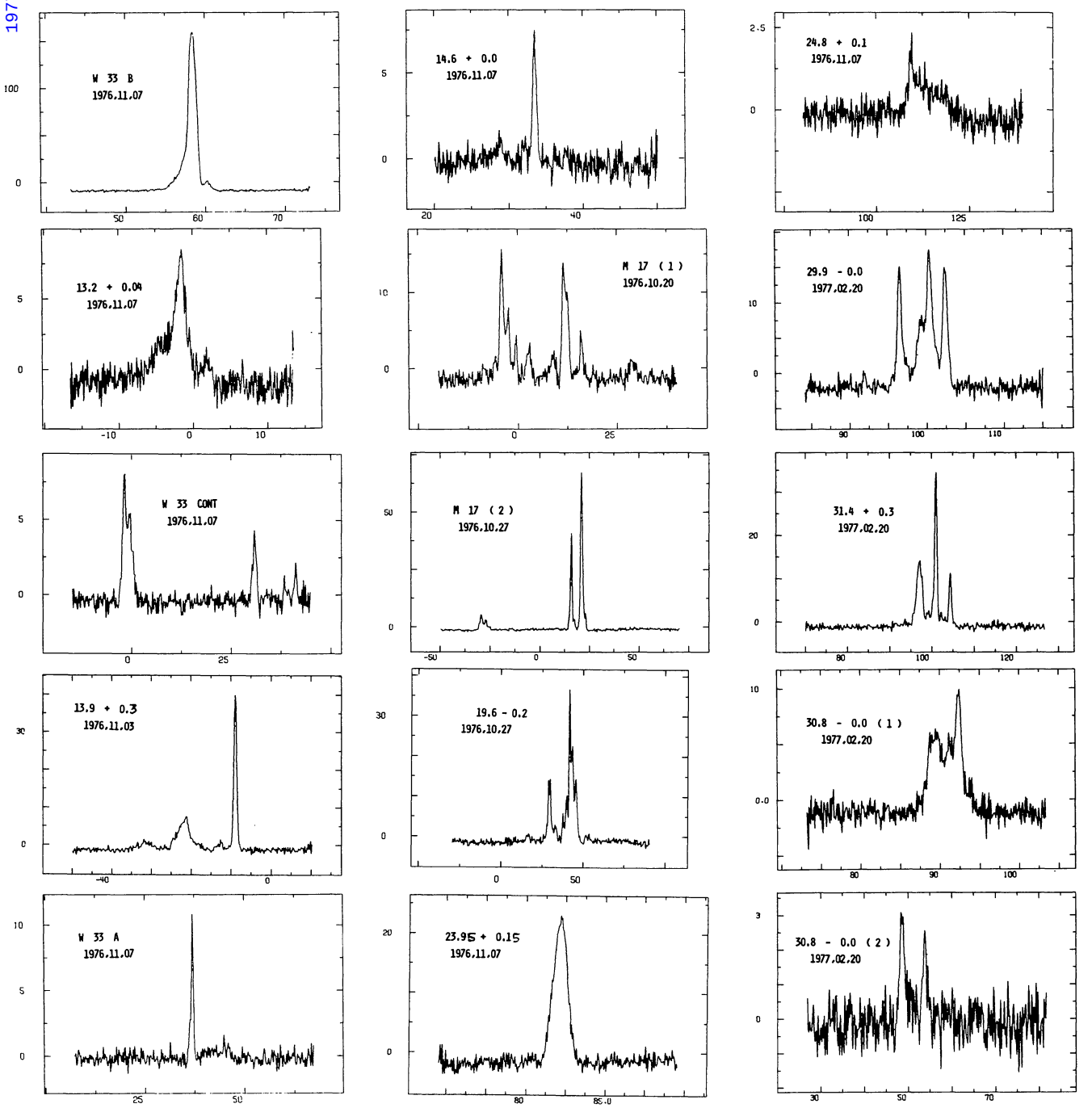

Figure 3

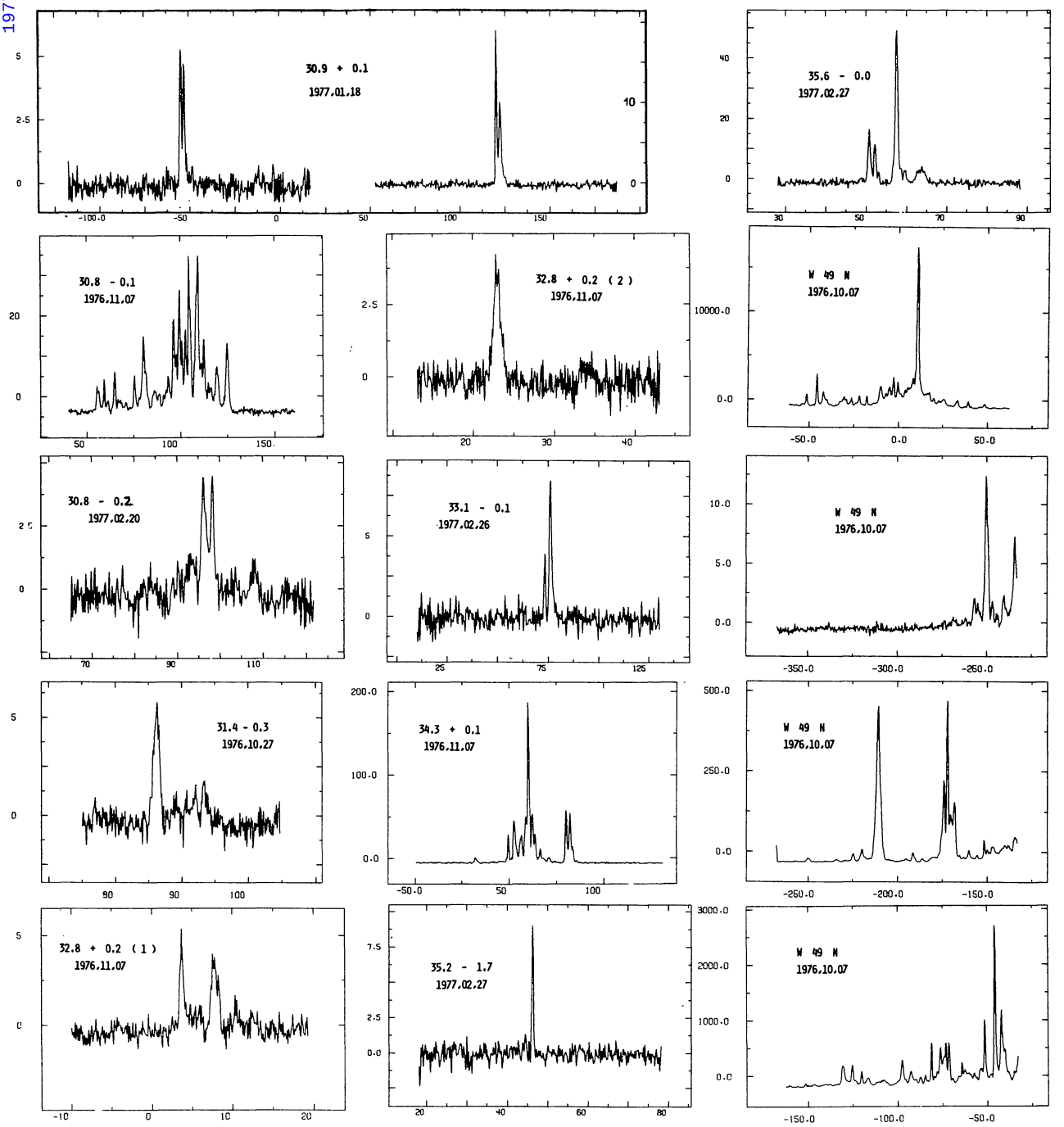

Figure 4

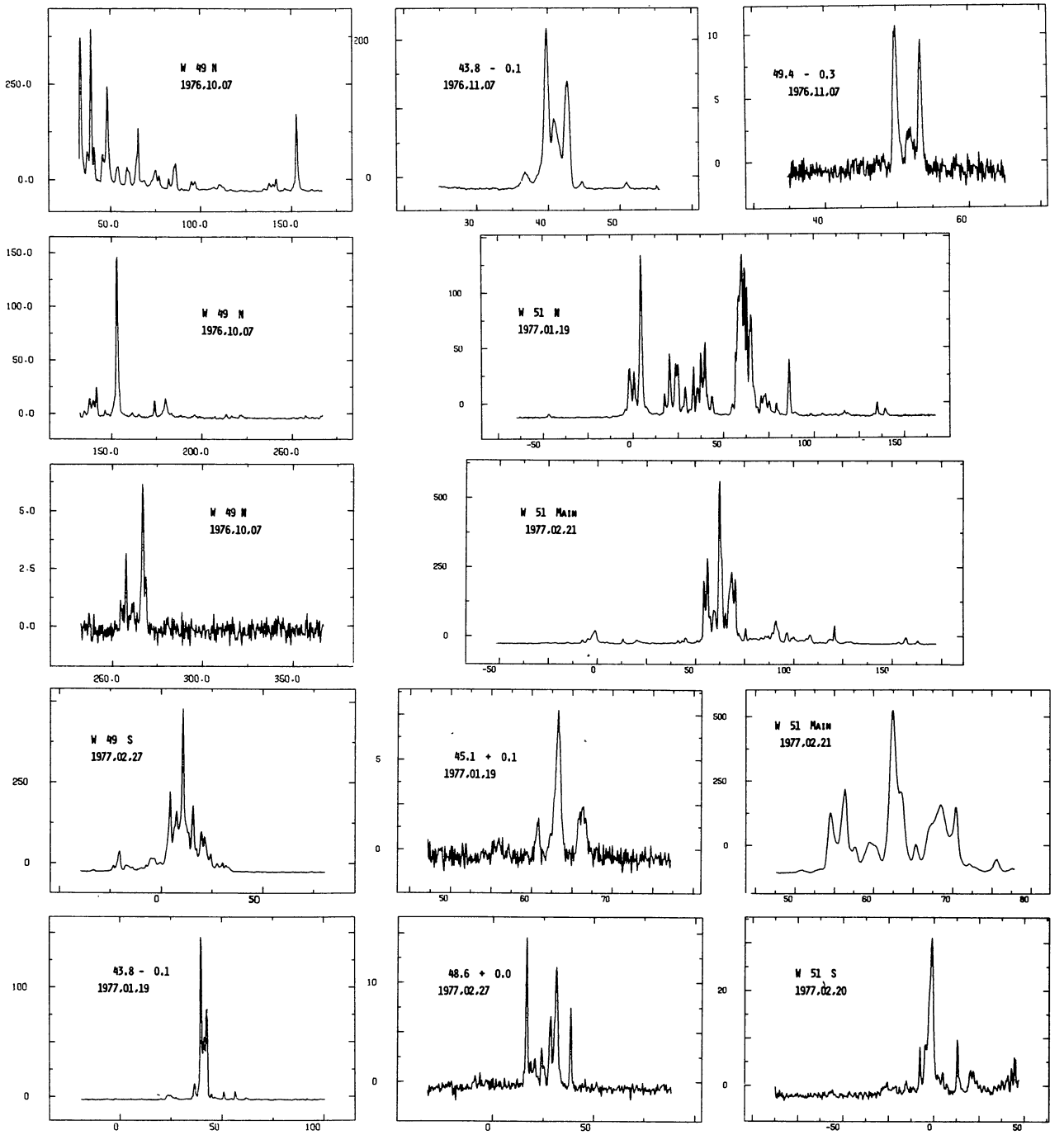

Figure 5

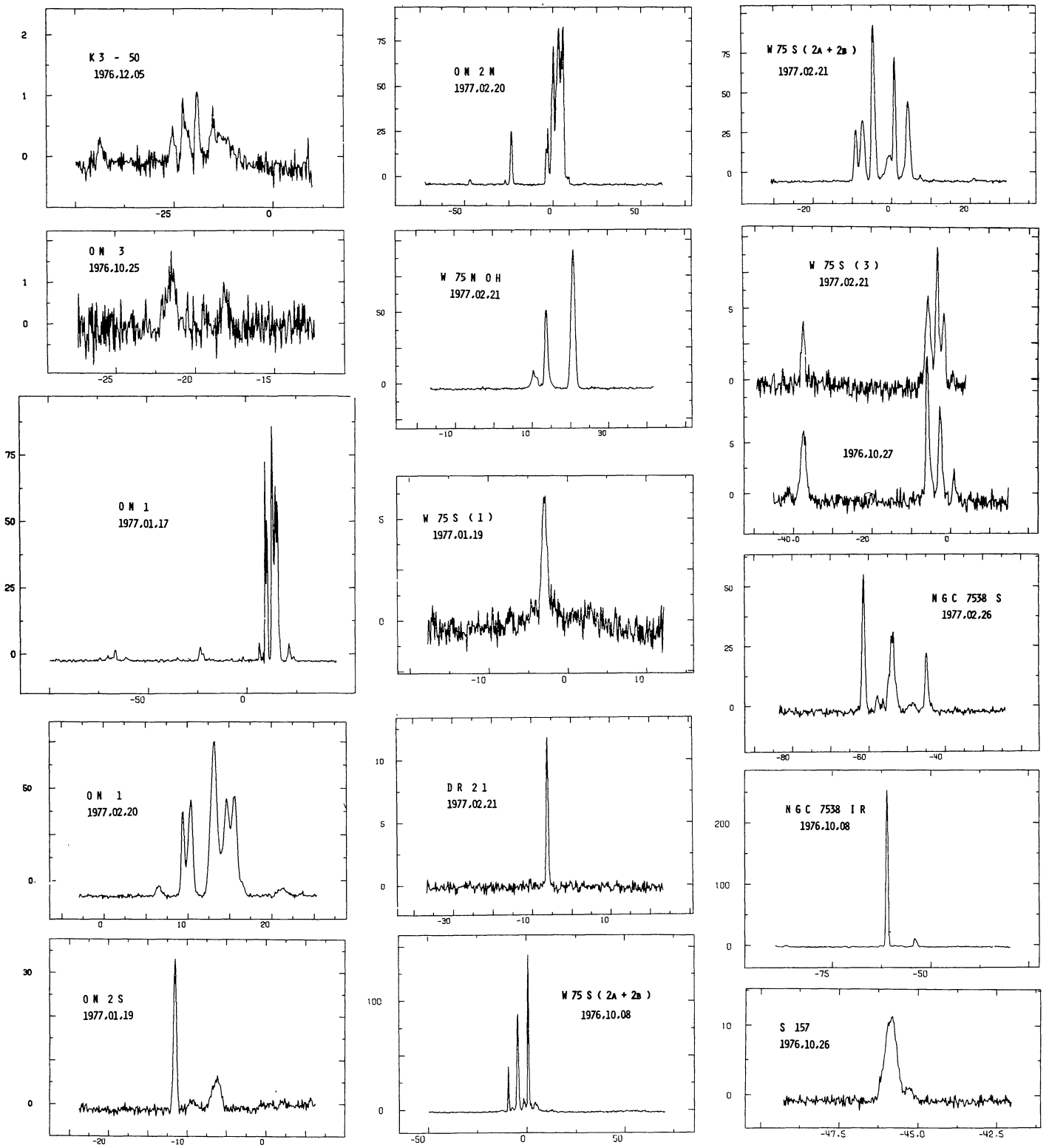

Figure 6

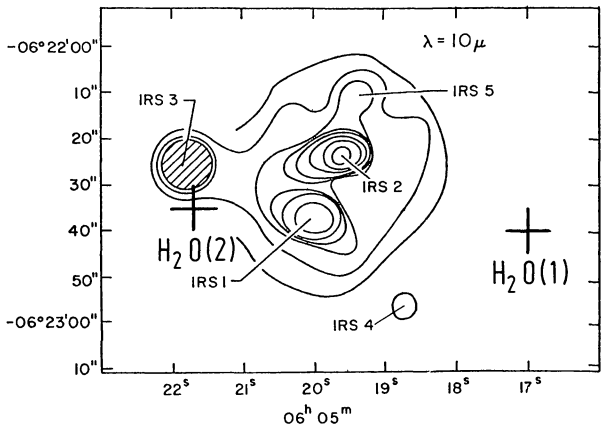

Figure 7 H_2O sources in Mon R2. The crosses show the absolute positional uncertainty for the two H_2O masers, relative to the 10 μ infrared contour map of Beckwith *et al.* (1976).

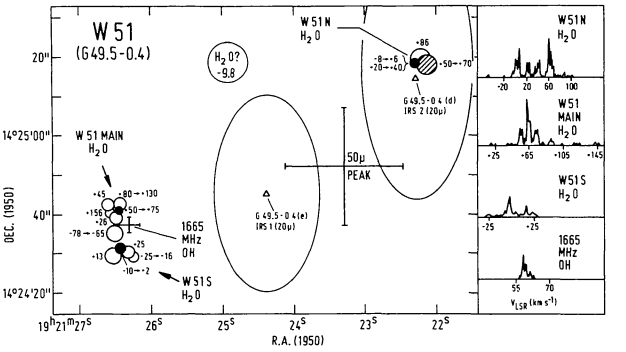

Figure 9 Maser line sources in W51, component G49.5–0.4. The small solid circles indicate the relative positional error for the individual H_2O features with the velocities indicated, in $km\,s^{-1}$. Shaded circles denote the strongest features. Ellipses show the half-power widths of the radio continuum sources (Martin 1972). Small triangles denote radio continuum and near infrared peaks (Wynn-Williams *et al.* 1974a). The 50 μ peak (Harvey *et al.* 1977) and OH position (Raimond and Eliasson 1969, Wynn-Williams *et al.* 1974b) are shown as crosses. The inset shows the approximate relative shapes of the maser spectra.

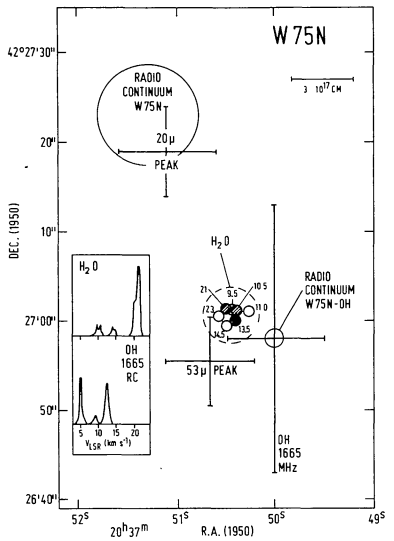

Figure 10 Infrared, radio continuum and maser line sources in the W75N region. The dashed circle shows the absolute uncertainty in the H_2O position, and the scatter in the cluster of small circles indicates the relative positional uncertainty for individual H_2O features with the velocities indicated ($km\,s^{-1}$). Shaded circles denote the strongest H_2O features in the fall of 1976. Infrared positions are from Wynn-Williams *et al.* (1974a) and Harvey *et al.* (1977), and the OH position from Hardebeck (1972). For the radio continuum source W75N, the circle indicates the approximate extent of the continuum emission (Harris 1974, Habing *et al.* 1974); for the radio continuum point source W75N–OH, the circle gives the positional uncertainty (Matthews *et al.* 1977). The linear scale (upper right) is for an assumed distance of 3 kpc. The inset shows approximately the relative shape of the H_2O lines in the fall of 1976, as well as those in the right circularly polarized spectrum of OH (Yngvesson *et al.* 1975).

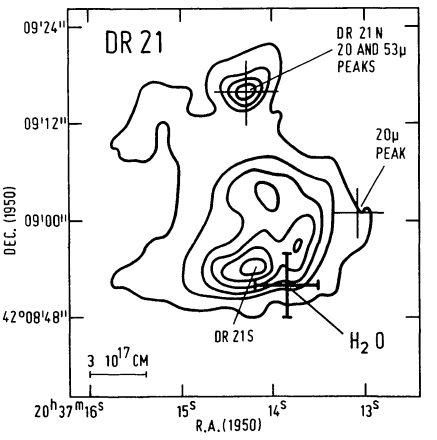

Figure 11 Position of the H_2O maser relative to the infrared and radio continuum peaks in DR21. The heavy cross shows the absolute positional uncertainty of the H_2O, the light crosses those of the infrared peaks (Wynn-Williams *et al.* 1974a, Harvey *et al.* 1977). Radio contours (Harris 1973) begin at $T_b = 392$ K and increase in steps of 784 K. The linear scale (lower left) is for an assumed distance of 3 kpc.

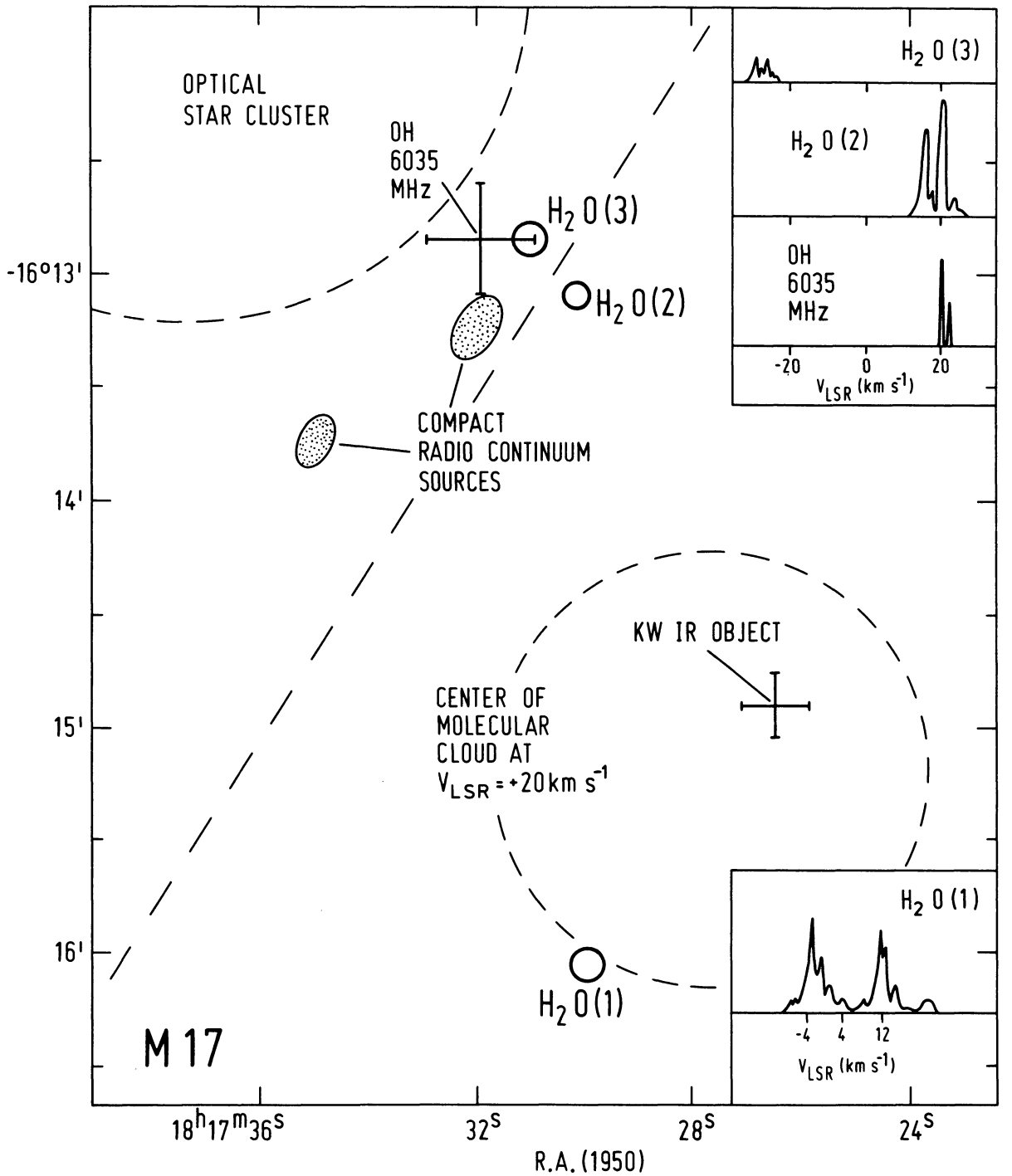

Figure 8 Maser line sources in M17. The small solid circles show the absolute positional uncertainty for the three H_2O sources. The OH position and spectrum at 6035 MHz are from Knowles *et al.* (1976). Positions and half-power widths (ellipses) of the compact radio continuum sources are from Webster *et al.* (1971). The extent of the optical star cluster was estimated from the data of Beetz *et al.* (1976). The diagonal dashed line shows roughly the half-power contour of the CO distribution, the centroid of which is shown by the dashed circle (Lada 1976). "KW" refers to the compact infrared source found by Kleinmann and Wright (1973). The inset shows approximately the relative intensities of the H_2O features in the fall of 1976.

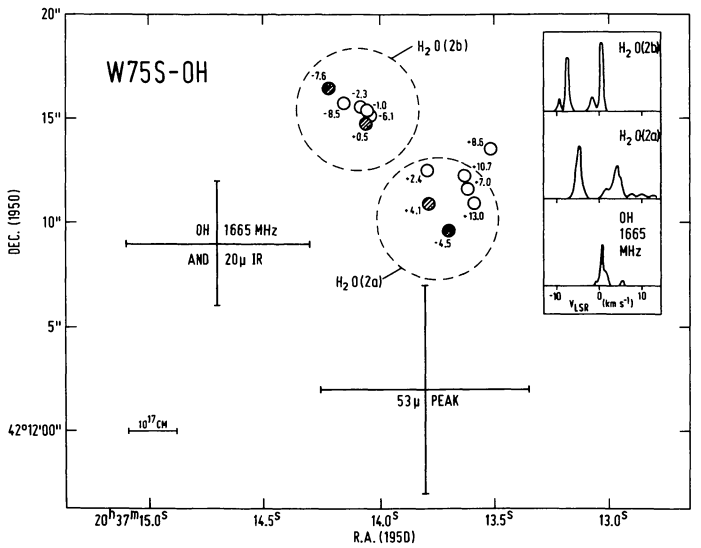

Figure 12 Maser line sources and infrared peaks near W75S–OH. Dashed circles show the absolute positional uncertainty in the two H_2O sources. The small circles give the positions measured for individual H_2O lines at the velocities ($km\,s^{-1}$) indicated. The scatter in the clusters of small circles probably indicates the relative positional uncertainty. Shaded circles denote the strongest H_2O features in the fall of 1976. Infrared positions are from Wynn-Williams *et al.* (1974a) and Harvey *et al.* (1977). The linear scale (lower left) is for an assumed distance of 3 kpc. The inset shows approximately the relative shapes of the H_2O spectra in Fall 1976, and that of the OH source (Raimond and Eliasson 1969).

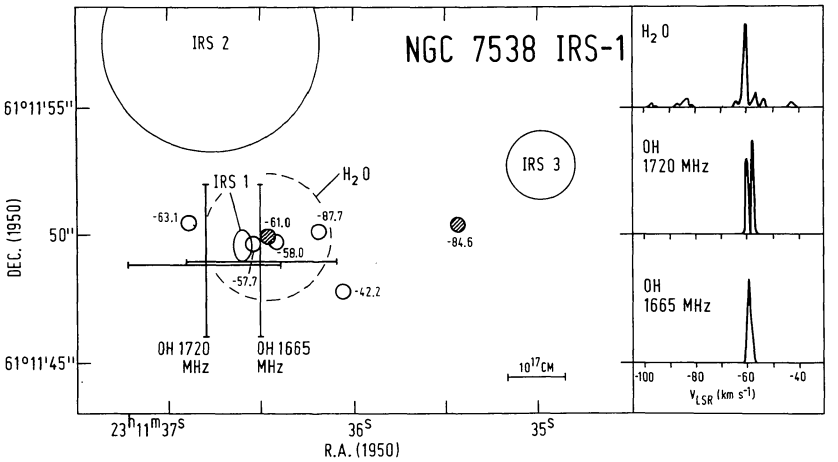

Figure 13 Continuum and maser line sources near NGC 7538–IRS 1. The dashed circle shows the uncertainty in the absolute position of the main H_2O line. Small circles show the positions measured for individual H_2O features at the indicated velocities ($km\,s^{-1}$). The scatter in these points probably corresponds to the relative positional uncertainty of the weaker features. Shaded circles denote the strongest features in the fall of 1976, The positional displacement of the feature at -84.6 $km\,s^{-1}$ is probably real, since it repeats itself on independent maps. The 20 μ infrared sources IRS 1, 2 and 3 (Wynn-Williams *et al.* 1974a, Willner 1976) correspond to the radio continuum sources (Martin 1973, Israel *et al.* 1973, Wink *et al.* 1975, Harris and Scott 1976). OH positions are from Wynn-Williams *et al.* 1974b). The inset shows the relative shapes of the H_2O spectra and the OH (Gruber and de Jager 1976). The linear scale (lower right) is for an assumed distance of 3.5 kpc.

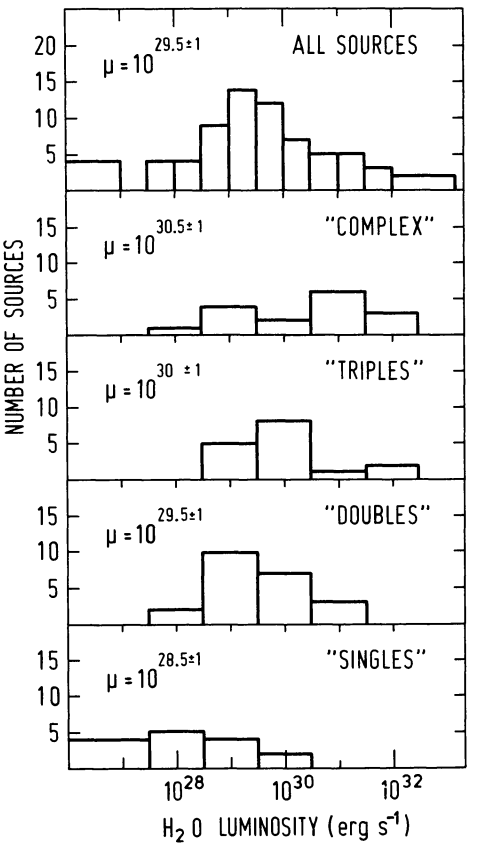

Figure 15 Luminosity function for H_2O sources. Vertical scale is linear, horizontal scale logarithmic. The H_2O luminosity is an approximate integral over all lines observed in the fall of 1976, and the masers were assumed to radiate isotropically. The uppermost distribution is the luminosity function for all H_2O sources in table 1 with known distances. The histograms underneath are the luminosity functions for the different classes of H_2O spectra described in the text. The median luminosity (erg s^{-1}) for each distribution is given at left, together with its standard deviation.

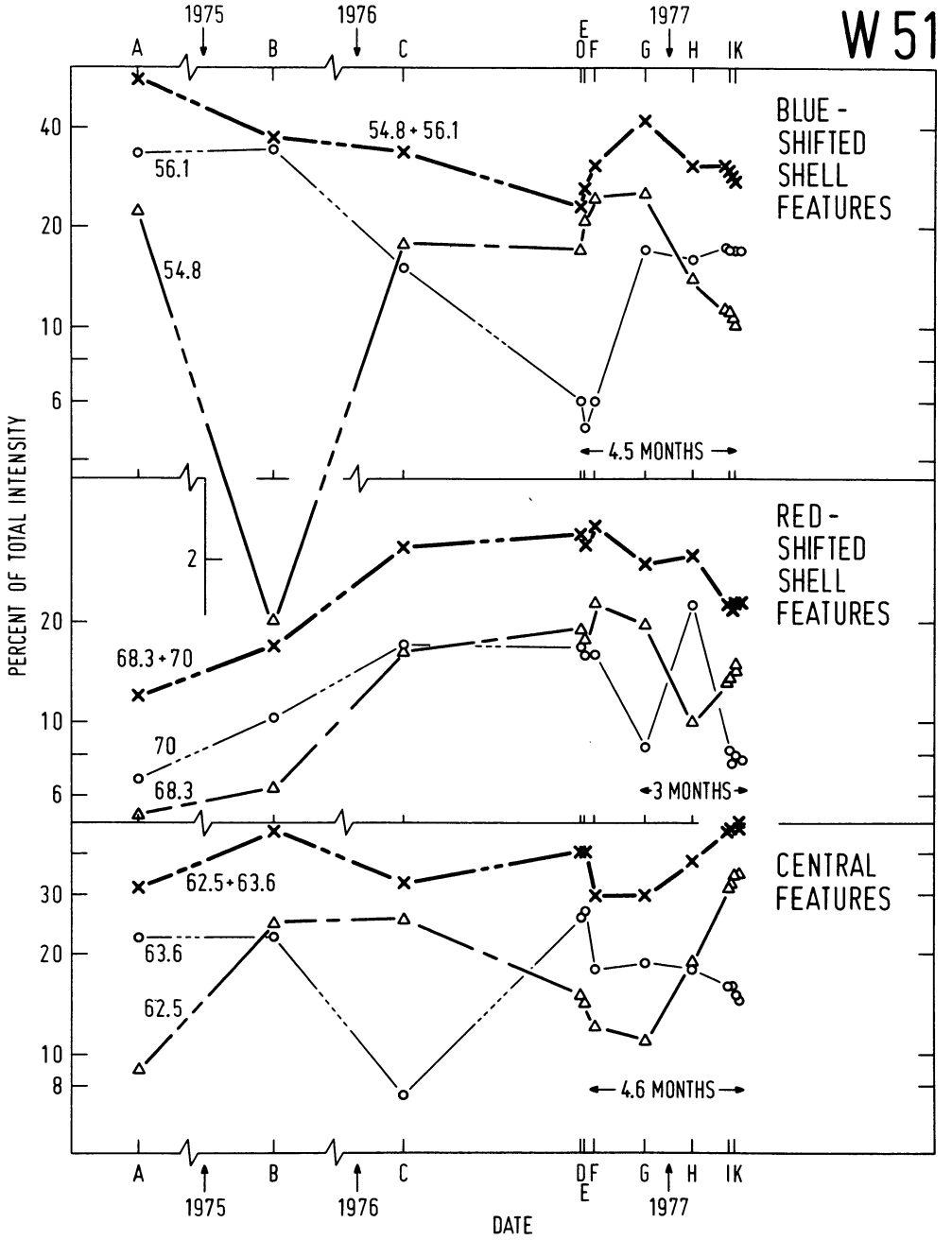

Figure 16 Relative intensity variations of selected H_2O features in W51 Main. The features are the two prominent sub-lines of each group of the "triple"-peaked structure in the spectrum. Note the interruptions in the time axis. Dates of observation (year, month, day) are A: 74 02 15 (Cato *et al.* 1976), B: 75 05 30 (Goss *et al.* 1976). Dates in 1976–77 (our data): C: 76 05 03; D: 76 10 09; E: 76 10 10; F: 76 10 20; G: 76 12 06; H: 77 01 19; I: 77 02 20/21; K: 77 02 26/27. Dashed lines indicate large gaps in the observations. The radial velocities ($km\,s^{-1}$) of the H_2O features are indicated at left. The intensities have been normalized to the total H_2O intensity of W51 Main on the dates of observation to reduce the effects of extinction and pointing errors. The total intensity is of the order of 10^4 Jy. The intensity scale is logarithmic to emphasize the percent change for a given feature. The sum of intensities for each pair of features is also given, and is labeled 54.8+56.1, etc. The uncertainties in individual relative intensity measurements are at most 10% of the normalized values. The time scales below the 76–77 data indicate roughly the periods between inflection points in the variations.

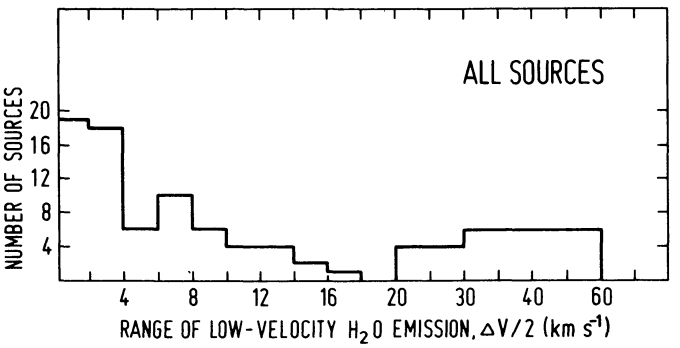

Figure 14 Number of H_2O sources as a function of the half-range, $\Delta V/2$, of the low-velocity emission. $\Delta V/2$ is probably the expansion velocity of the circumstellar shell. The histogram includes all 82 sources in our sample. Note the compression in the horizontal scale for velocity half-ranges ≥ 20 km s^{-1}.

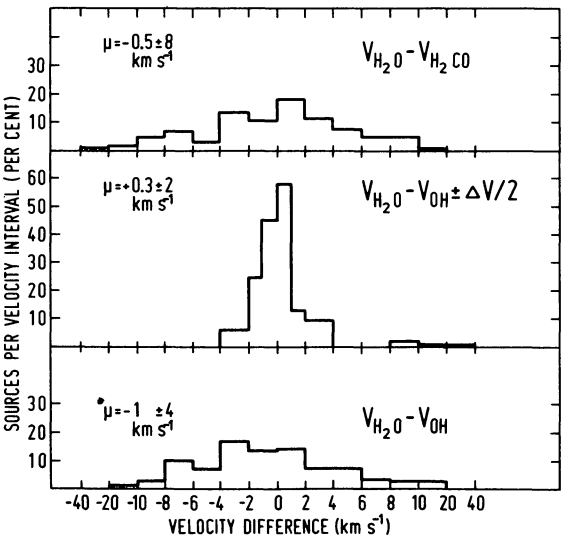

Figure 18 Comparison of the velocities of H_2O sources, OH sources and molecular clouds (H_2CO lines). The upper and lower plots are the number of sources per velocity interval (expressed as per cent of the sample) are plotted against the differences between V_{H_2O}, the centroid of the H_2O spectrum, and the velocities of OH and H_2CO (lower and upper diagrams). The middle histogram limits the sample to those H_2O sources with single lines or with symmetrical spectra; the difference has been taken between V_{OH} and the true velocities, $V_{H_2O}\pm\Delta V/2$, of the H_2O lines. Note the compression of the velocity scale beyond ± 10 km s^{-1}.

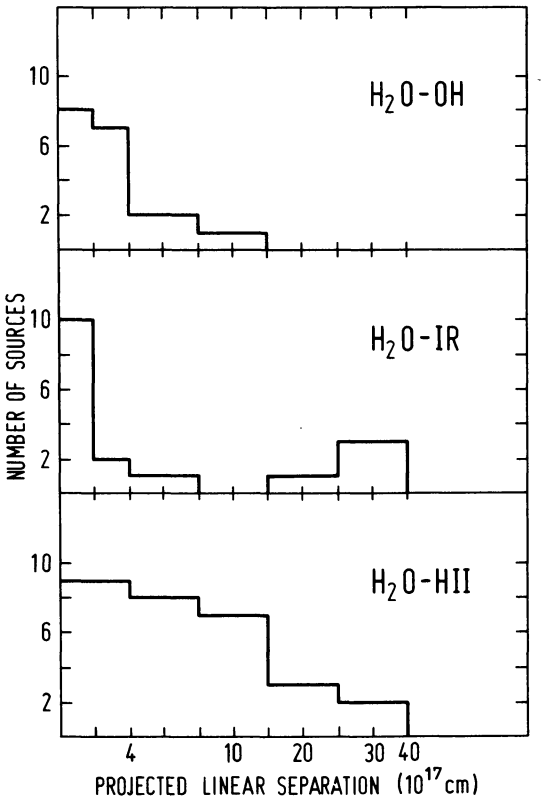

Figure 17 Histogram of the projected linear separation between H_2O masers and: OH sources (upper), compact infrared sources (middle) and radio continuum sources (lower). Vertical scale is linear, horizontal scale is linear to 10^{18} cm, compressed thereafter. Only interferometric positions for OH sources and HII regions were used. Sources were counted only if the net error in the angular separation was $\leq \pm 8''$. The separations between H_2O and OH positions have the largest uncertainties.

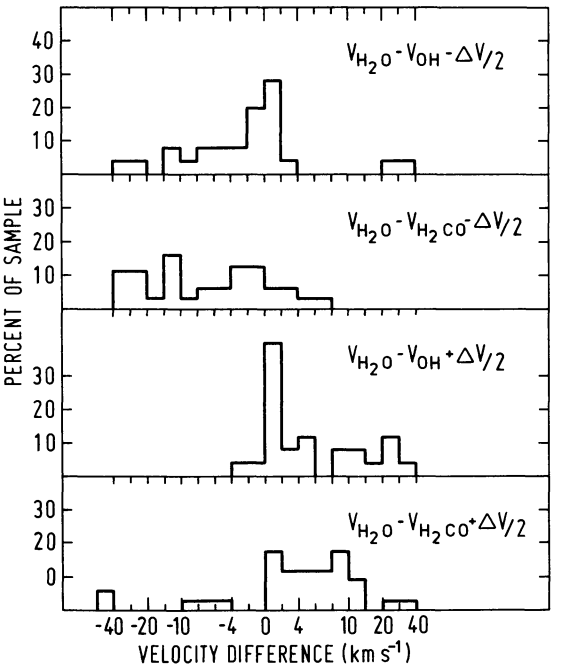

Figure 19 Correlation of the OH and H_2CO velocities with the red- and blue-shifted H_2O velocities (same sample as in figure 18, middle). These histograms test in an unbiased manner the correlation of H_2CO and OH lines with the red- and blue-shifted parts of the circumstellar shells, represented by the H_2O velocities $V_{H_2O}+\Delta V/2$ and $V_{H_2O}-\Delta V/2$, respectively.